FORMATION EVALUATION USING WAVELET ANALYSIS ON LOGS OF THE CHINJI AND NAGRI FORMATIONS, NORTHERN PAKISTAN

A Thesis

by

EMRE DORUK TANYEL

Submitted to the Office of Graduate Studies of
Texas A&M University
in partial fulfillment of the requirements for the degree of

MASTER OF SCIENCE

August 2006

Major Subject: Petroleum Engineering

FORMATION EVALUATION USING WAVELET ANALYSIS ON LOGS OF THE CHINJI AND NAGRI FORMATIONS, NORTHERN PAKISTAN

A Thesis

by

EMRE DORUK TANYEL

Submitted to the Office of Graduate Studies of
Texas A&M University
in partial fulfillment of the requirements for the degree of

MASTER OF SCIENCE

Approved by:

Chair of Committee,	Jerry L. Jensen
Committee Members,	Brian J. Willis
	Thomas A. Blasingame
Head of Department,	Stephen A. Holditch

August 2006

Major Subject: Petroleum Engineering

ABSTRACT

Formation Evaluation Using Wavelet Analysis on
Logs of the Chinji and Nagri Formations, Northern Pakistan. (August 2006)
Emre Doruk Tanyel, B.S., Middle East Technical University, Turkey
Chair of Advisory Committee: Dr. Jerry L. Jensen

The relatively new method of using wavelets in well log analysis is a powerful tool for defining multiple superimposed scales of lithic trends and contacts. Interpreting depositional processes associated with different scales of vertical variation within well log responses allows prediction of the lateral extent of sands and the distribution of internal flow barriers important for development of oil field recovery strategies.

Wavelet analysis of grain-size variations in a 2.1 km thick fluvial section including the fluvial Chinji and Nagri Formations, northern Pakistan, revealed three major wavelengths. Reliability of the wavelength values was tested and confirmed by multiple sectioning of the dataset. These dominant wavelengths are interpreted to reflect vertical variations within individual channels, the stacking of channel belts within overbank successions due to river avulsion, and larger-scale channel stacking patterns within this foreland basin that may reflect allocyclic influences. Wavelet analysis allows quantification of the scales of periodic vertical variations that may not be strictly cyclic in nature.

Comparison of total wavelet energies over all scales for each depth to the grain size and sand percentages yielded good correlations with sand proportion curves. Although changes in the wavelet energy profile were much more distinct with respect to grain size, lithic boundaries' locations were not detected based solely on the total of the wavelet energies.

The data were also analyzed using Fourier transforms. Although Fourier transforms of the data yielded the smallest scale cyclicities, the higher-order cyclicities

were not defined. This comparison demonstrates the power of wavelet analysis in defining types of repetitive, but not strictly cyclic, variations that are commonly observed in the sedimentary record.

Assessments of Milankovitch cyclicities were performed for the Chinji and the Nagri Formations using statistical and analytical analysis methods. A clear match between Milankovitch frequency ratios and vertical lithic variations was not observed, and thus distinct climatic control on cyclic lithological trends was not demonstrated.

Analysis using wavelets to determine wavelet coefficients helps quantify characteristic scales of vertical variations, cyclicities, zone thicknesses, and locations of abrupt lithic boundaries. Wavelet analysis provides methods that could be used to help automate well log analysis.

DEDICATION

To my sister, my father, and my mother

ACKNOWLEDGEMENTS

First and foremost, I would like to express my deep and sincere gratitude to my advisor Dr. Jerry L. Jensen, for his support throughout all stages of this study. I received valuable comments and motivation during the discussions we had. He was always there when I needed guidance, and his approach to the problems I faced throughout the study has influenced me to become a better engineer.

I also wish to express my warm and sincere thanks to Dr. Brian J. Willis for the time and effort he has put into the study. His involvement has helped me greatly in understanding the reality of the problem and his excellent geologic knowledge of the area has had great influence on the direction this study took in search of answers.

I would like to thank Dr. Thomas A. Blasingame, the experience I gained from the courses I have taken from him has helped me in developing a perspective for data analysis.

I also would like to thank TPAO for their sponsorship and their support which enabled me to complete my graduate studies. Their support has given me the chance to fulfill my lifelong dream of having an advanced engineering education.

TABLE OF CONTENTS

CHAPTER Page

LIST OF FIGURES

FIGURE Page

FIGURE Page

LIST OF TABLES

CHAPTER I
INTRODUCTION

1.1 Problem

The kilometers thick Siwalik Group of the Himalayan foredeep basin is a wedge of fluvial deposits shed from the rising Himalayan mountain belt. These strata have long been described as cyclic. Vertical lithic variations occur at a variety of scales from meter-thick sandstone-mudstone interbeds to kilometer-thick alterations between sandier and muddier formations. Although different scales of vertical lithic trends have been described and interpreted in terms of depositional process, complex superposition of deposits formed by different depositional mechanisms makes it difficult to define characteristic scales of different types of lithic trends and to separate systemic trends from random variations. This is particularly true for larger scales of lithic variation, defined not by simple lithic interlayering but rather by a complex clustering of different types of lithic bodies.

An alternative approach to detailed facies interpretation is to apply different methods of signal processing to define lithic trends and repetitive scales of lithic variation. Geological signals that can be represented in a depth or time series can resist analysis by standard signal processing techniques that assume a superposition of perfectly cyclic variations. Variation in these records may not be stationary and dominant cyclicities can vary in frequency and amplitude over the length of record. This problem can be overcome by applying methods using wavelets in log analysis.

This thesis follows the style and format of *Petrophysics*.

Wavelet analysis was performed on grain size log measurements collected at 1m intervals over a 2100m section of the Siwalik Group to identify periodic vertical patterns within the Chinji and Nagri Formations and to interpret these patterns in terms of the nested influence of different-scale depositional controls. Methods of wavelet analyses follow those used in well log analysis of the Egret Member eastern Canada (Prokoph and Agterberg, 2000) and the Ormskirk Sandstone, Irish Sea (Rivera et al., 2004).

1.2 Relevance to Reservoir Characterization

Reservoir characterization studies provide a basis for reservoir management and planning. Therefore an effective analysis of the data may be critical for an effective reservoir characterization study in order to provide the best information possible. The rapid development of technology for gathering and storage of petrophysical and engineering data has made reservoir characterization an immense task. It would be advantageous to develop methods that deal more effectively with these data by automated processing to reduce analysis time. This requires not only efficient application of the known techniques but also close monitoring and implementation of recently developed methods, when available. One such advance that can be useful in reservoir characterization studies is the wavelet transform signal analysis technique. Although the wavelet transform has been around for some time (since 1909), the power of wavelet transforms has been unappreciated until recently, when Morlet used wavelets in seismic interpretation studies as a mechanism to work in the time-frequency domain and overcome difficulties resulting from the frequency dependent nature of seismic waves (Morlet et al., 1982a, b).

Geological data, which provide the basis for many petroleum characterization studies, are also transitional, making them a good candidate for wavelet analysis. One of the aims of this study is to introduce analysis of geological data as a possible application for wavelets in the petroleum industry and encourage use of wavelets in other studies of this field. For example, wavelet-based determinations of geologic boundaries and factors

controlling depositional heterogeneities within reservoirs could enhance the examination of the well logs and other data. Interpreting depositional processes associated with different scales of vertical variation allows prediction of the lateral extent of sands and the distribution of internal flow barriers and is important for the development of oil field recovery strategies. Previous studies that used such an approach include work by Aniekwena et al. (2003) on Green Canyon 18 field, Gulf of Mexico. Their model distributed the facies based on the complex geometry of principal architectural elements,and captured the production and pressure histories better than previous studies of this field.

1.3 Brief Statement of Important Conclusions

Wavelet analysis performed on log data from the Chinji and Nagri Formations revealed three major wavelengths for each formation, where each wavelengths is related to multiple scales of channel stacking. There is a change in these three characteristic wavelength scales between intervals previously interrupted to be deposited by river systems of different scale. Smaller river systems of the Chinji Formation having been displaced by larger systems during the deposition of the Nagri Formation. While successfully detecting the channel thicknesses defined in previous qualitative studies for the Chinji Formation (where individual channel deposits were generally separated by overbank deposits), wavelet analysis was unable to distinguish channel thicknesses for the Nagri Formation (where many channels were erosionally superimposed). Wavelet analysis was successful in defining total sandstone body thicknesses of connected channel deposit clusters.

Boundary analysis revealed good correspondence between patterns from grain size and sand percentages. The sum of magnitudes of wave energies at each depth determined from wavelet analysis clearly revealed boundaries between major lithologic units.

Although Fourier transforms of the data successfully defined smaller-scale cyclicities, those Fourier transforms were not able to capture the level of detail of locations of these cyclicities and the magnitudes or positions of the higher level cyclicities. Assessment of vertical lithic patterns in terms of ratios of Milankovitch cyclicities using both statistical methods and analytical methods did not show a strong relationship-suggesting Milankovitch-driven climatic changes were not the dominant control on depositional cyclicities observed in these deposits.

1.4 Organization of the Thesis

Chapter I presents the problem, its relevance to reservoir characterization and points out the important conclusions. Chapter II is a literature review focused on the geology of the area and background information about wavelets with emphasis on their use in petroleum industry. After presenting the analysis methods in Chapter III, Chapter IV discusses results that were obtained. Chapter V presents a summary and conclusions, and Chapter VII proposes possibilities for future work.

CHAPTER II
LITERATURE REVIEW

2.1. Geology of Chinji and Nagri

The Chinji and Nagri Formations of the Siwalik Group are part of the orogenic clastic wedge in the Himalayan foredeep basin in northern Pakistan (Fig. 2.1). This basin began forming due to the collision of India and Eurasia, around 40-50 Ma and similar to other collision-related basins, it contains records of fluvial deposition adjacent to rising mountain belts induced by topographic load of the hanging wall (Willis, 1993a).

Figure 2.1 Map of the study area (from Willis, 1993a).

The 3-4 km thick, middle Miocene through Pliocene, Siwalik Group is divided into three sub-groups consisting of Lower, Middle and Upper Siwalik (Fig. 2.2). The Lower and the Middle-Upper Siwalik Group are upward coarsening megacycles (Kumar et al., 2003). Formations within the Siwalik Group are defined by variations in the proportion of channel sandstones to overbank deposits. Well documented records of sedimentologic changes are available, which provide unusually good information over the stratigraphic successions with hundreds of meters of vertical continuity. Correlations

of upsection lithologic trends based on magnetostratigraphy indicate that lithostratigraphic transitions are diachonous.

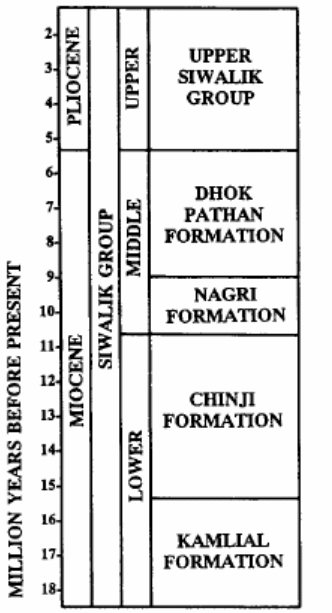

Figure 2.2 Lithostratigraphy of the Siwalik Group (from Willis, 1993a).

The best exposures of the Siwalik Group occur on the Potwar Plateau of northern Pakistan, where thrusting of strata along underlying salt beds have uplifted kilometers-thick outcropping successions. Vertical sections of Siwalik Group in this area record a long period of sediment progradation away from the rising Himalayan orogenic belt. Although a number of studies defined the depositional paleoenvironments and changing depositional rates for successions, these studies were mainly local and did not define basin scale lithic changes due to local complexities. Although evaluation of wider areas might provide a better definition of regional formations across the ancient Siwalik Basin, basin-scale patterns of deposition are generally considered to be analogous to those within the modern Himalayan foredeep.

On modern plains of the Himalayan foredeep multiple scales of rivers pass from the mountain belt and converge into major rivers on the Ganges plains toward the basin axis. Deposition is controlled by the location of large rivers exiting the mountain belt that

deposit low-gradient sediment fans extending up to 200 km into the basin. Sediment grain size, floodplain gradients, deposition rates, and braiding indices of channels decrease away from fan apices. Secondary systems of smaller rivers, with lower depositional rates, carry finer sediment loads in areas between the sediment fans deposited by the major river system. This analogy with modern drainage systems suggests that Siwalik Group channel sandstone proportion and the character of overbank sequences should vary both parallel to and away from the mountain belt. Depositional variations within this setting occur as river channels avulse across their fans, as floodplains of some river systems expand and displace other systems within the basin, and as extrabasinal controls like tectonism or climatic variations change the grain size of sediment entering the basin, regional sediment aggradation rates, and behavior of the rivers systems in terms of channel braiding, avulsion frequency, and overbank deposition patterns. Although these varying controls can each be periodic, they are not necessarily cyclic. This can make it difficult to separate and interpret influences of different scale processes on observed stratigraphic patterns. Qualitative definition of different scales of variation may be subjective, and even perfectly cyclic variations may be difficult to define where deposition rates vary significantly over time.

The Chinji and the Nagri Formations are composed of tens of meters of thick sandstone bodies deposited by large rivers that are separated by mudstone dominated overbank successions. The proportion of major sandstone bodies relative to mudstone-dominated overbank deposits increases from the Chinji Formation upwards into the Nagri Formation (Fig. 2.3) (Willis, 1993b). Sandstone bodies are composed of channel deposits vary from 5 m to 15 m thick within the Chinji Formation and can be as much as 30 m thick in the Nagri Formation (Willis and Behrensmeyer, 1995). The mean grain size of channel sandstones also increases upwards. Overbank successions are composed of variable amounts of minor meter-thick channel, levee and crevasse splay sandstones interbedded with mudstone intervals. Vertical aggradation rates, defined by paleomagnetic dating, increase by a factor of 3 within this upward-coarsening succession.

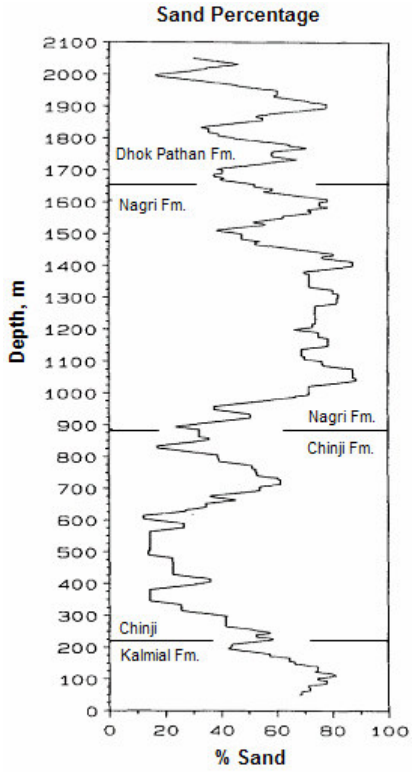

Figure 2.3 Upsection variation in the proportion of sandstone bodies relative to mudstone dominated successions (from Willis, 1993b).

Smaller scale lithic variations within individual channel deposits reflect episode deposition over multiple river floods. Overbank successions also have a complex internal architecture, related to shifting depositional environments and processes on floodplains. Although it is generally assumed overbank deposition is a gradual vertical aggradation of sediments from suspension following flood, the overbank sequences of the Chinji Formation suggest that patterns of sediment aggradation on these ancient floodplains were episodic, with periods of rapid deposition extending for at least several kilometers followed by long hiatuses and development of soils (Willis and Behrensmeyer, 1994).

The major sandstone bodies have a complex arrangement of internal channel deposits. Individual channel deposits fine upward, reflecting the sorting of grains within migrating rivers. Major sandstone bodies are not randomly distributed within the vertical section; they appear in vertically interconnected clusters on a scale of tens to 100 m thick,

separated by intervals dominated by overbank deposits with fewer isolated sandstone bodies.

Paleochannel reconstructions of the Chinji Formation show that individual channel-segments typically had widths of 80-200 m and depths of 4-13 m. These channels had belt widths of 1-2 km and braiding indices of 2-3. Nagri Formation deposits, in contrast, had widths of 200-400 m and depths of 15-30 m. They were also braided with belt widths of 5 km (Willis, 1993a). Sedimentologic interpretations suggest the Chinji and Nagri Formations reflect deposition by two river systems, a smaller river system (discharge ~1500-2000 m^3/s) deposited the Chinji Formation, and a larger river system (discharge ~ 3000-5000 m^3/s) deposited much of the Nagri Formation.

Although cyclic patterns of deposition have long been reported to occur within the Siwalik Group (as well as within most other fluvial successions), the range of superimposed lithic variation makes it hard to define distinct periodic or cyclic patterns and characteristic scales related to depositional mechanisms. Periodic trends within this succession have previously been interpreted to reflect specific-scale depositional controls based on detailed sedimentologic study, ranging from autocyclic shifts in deposition to potentially allocyclic extrabasinal processes. The aim of this study is to use an alternative more quantitative approach to define the cyclicities by performing wavelet analysis for assessment of logs from the Siwalik Group.

2.2 Wavelets

2.2.1 Introduction to Wavelets

The term “wavelet” refers to a small wave. Wavelets are oscillating functions that are non-zero over a limited duration, are zero elsewhere, with an average value of zero over the entire domain. Wavelets can be shifted forward or backward in time and/or stretched or compressed in time. This characteristic allows wavelets to keep track of frequency and time information by separating the signal into distinct frequency packets that are

localized in time domain (Fig. 2.4). Thus, wavelets can be used for detecting both abrupt changes and longer-term patterns in the signal that may be cyclic or simply repetitive in scale.

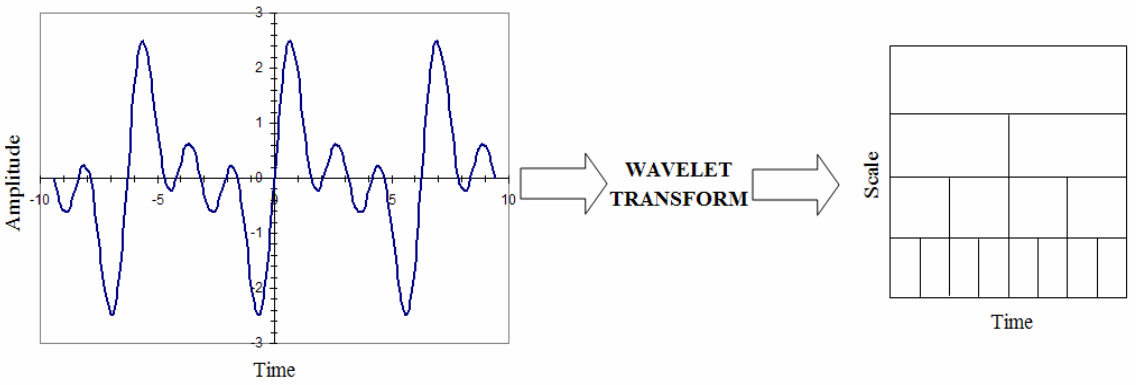

Figure 2.4 Graphical description of wavelet transform.

The introduction in 1909 by the Hungarian mathematician Alfred Haar of a function called the "Haar Wavelet" (Fig. 2.5) was the birth of the concept of wavelets (Mackenzie, 2001). This first and perhaps the simplest type of wavelet is a step function, formed of a short positive pulse followed by a short negative pulse. Approximations of signals generated using the Haar wavelet are rough due to its discontinuous nature.

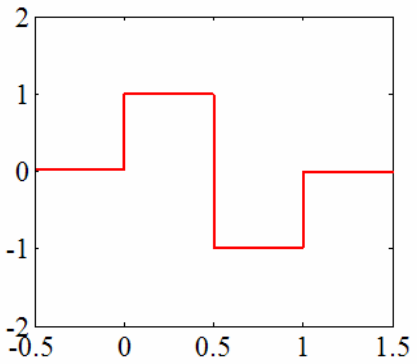

Figure 2.5 Haar wavelet.

Wavelet analysis techniques were not widely used until recently, as wavelets were generally a topic known to only a few with special interest in signal processing. The re-

discovery and development of wavelets is mostly a result of the search of scientists to overcome the deficiencies of the Fourier Transform (FT). The FT (Fig. 2.6), introduced in the 1920's by the French mathematician Joseph Fourier, is probably the most widely used technique in signal analysis. It involves decomposing a time-dependent signal into its various orthogonal frequency components using the sine and cosine functions that oscillate n times per 2π interval (Boggess and Narcowich, 2001). The FT generates a frequency domain representation of the analyzed function as

$$F(\omega) = \int f(t) e^{-j\omega t} dt \tag{2.1}$$

where *f(t)* is the function to be analyzed, ω is the frequency, *t* is time or position, and *j* $= \sqrt{-1}$

The FT has proved to be a very powerful tool in determining the characteristics of signals that are cyclic and stationary over time. Such transform relate strengths to characteristic superimposed sine and cosine functions. This technique averages local frequency information in the signal to define frequency domains at the expense of local information about locations of particular events. Music synthesizers that replicate sounds of instruments as combinations of pure sine and cosine waves are an example of this phenomenon. Transforms define notes, but they can not match the actual playing of instruments perfectly because playing an instrument contains transient features that, at best, can be poorly imitated by sine waves (Mackenzie, 2001).

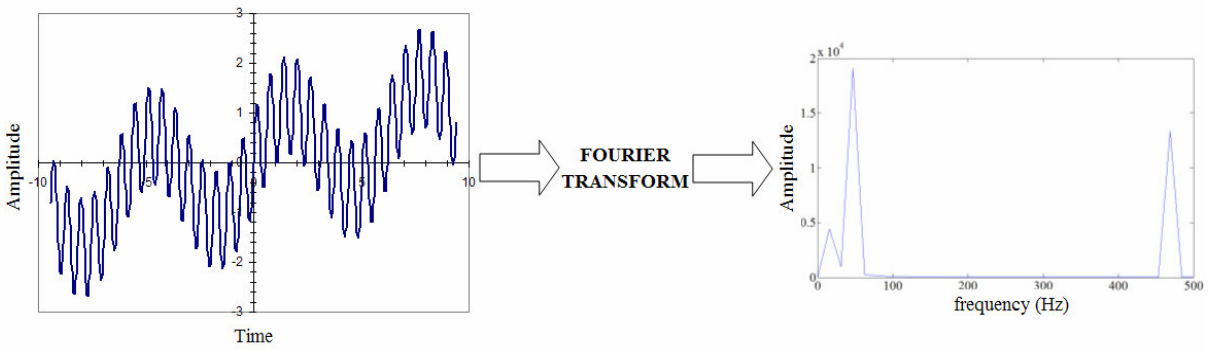

Figure 2.6 Graphical description of Fourier transform.

One approach to overcome this deficiency of the FT was to use a variable size windowed FT, where a window size is selected and the FT is calculated within the window while sliding the window along the time axis. This method is a tradeoff between the time and frequency information. The transform is highly dependent on the window size selected. The selected window remains the same for all frequencies and at low frequencies the frequency localization is lost and for windows of high frequencies the time localization is lost. This problem is similar to the Heisenberg Uncertainty Principle, which was originally applied to momentum and location of moving particles (Loughlin et al., 1992). In 1927 Werner Heisenberg stated that the velocity and position of an object cannot both be measured at exactly the same time. In signal processing terms this indicates time-frequency representation of a signal can not be determined, (i.e. one cannot precisely determine at what time instance a frequency component is located). This is mathematically defined as,

$$\Delta t \Delta f \geq \frac{1}{4\pi} \tag{2.2}$$

where Δt and Δf represent the time and frequency resolutions respectively.

Wavelets became popular in the 1980s after Jean Morlet, an engineer working for Elf-Aquitaine, used the function today called the Morlet Wavelet (Fig. 2.7) instead of the FT in his geologic studies to analyze seismic surveys (Guan et al., 2004). His analyses, in a similar fashion to the windowed FT with a changing window width to decompose the time series to time-frequency space, computed the transform for every spectral component. Seismic data contains many transients and abrupt changes recorded as the wave travels from one layer to another. Information on the location of rock layers are contained in these transients. Morlets work showed that, in contrast to the FT, wavelets are better suited for analysis of signals that are not strictly cyclic and wavelets contain nonstationary or transitory characteristics due to their finite duration.

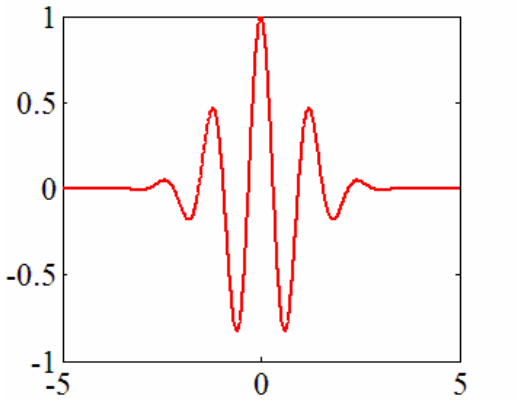

Figure 2.7 Morlet wavelet.

Wavelets are constructed using a function $\psi(t)$, the "mother wavelet", confined to a limited interval decreasing rapidly to zero as $|t|$ tends to infinity. In other words, wavelets must be compact and must satisfy

$$\int_{-\infty}^{\infty} \psi(t) = 0 \tag{2.3}$$

$\psi(t)$ is an archetype that can be used to define individual wavelets. There are a number of different types of mother wavelets available in the literature, where the wavelet is selected according to the type of data to be analyzed. Generated wavelets using the mother wavelet are shifted and scaled versions of the mother wavelet, and are defined by:

$$\psi_{a,b}(t) = \frac{1}{\sqrt{a}} \psi\left(\frac{t-b}{a}\right) \tag{2.4}$$

The wavelet transform decomposes the time series into a time-frequency space and generates wavelet coefficients, which are also functions of scale and position by comparing the shifted and scaled versions of the wavelet projected on to the signal.

$$C(a,b) = \frac{1}{\sqrt{a}} \int_{-\infty}^{\infty} f(t) \psi^* \left(\frac{t-b}{a}\right) dt \tag{2.5}$$

Thus, the wavelet acts as a window function which can be used for multi-resolution analysis (MRA) of a signal at different frequencies with different resolutions. The size of the window is increased in space by increasing the scaling parameter *a*, thus covering longer wavelength cyclic components in *f(t)*. The parameter *b* defines the location of the

wavelet window along the space axis. Mathematically, a delay of b to the function $f(t)$ can be represented by $f(t-b)$. Therefore, by changing the parameters a and b, $C(a, b)$ can be calculated over the entire location-wavelength plane (Fig. 2.8). These coefficients are based on degree of similarity, thus a larger coefficient means greater similarity.

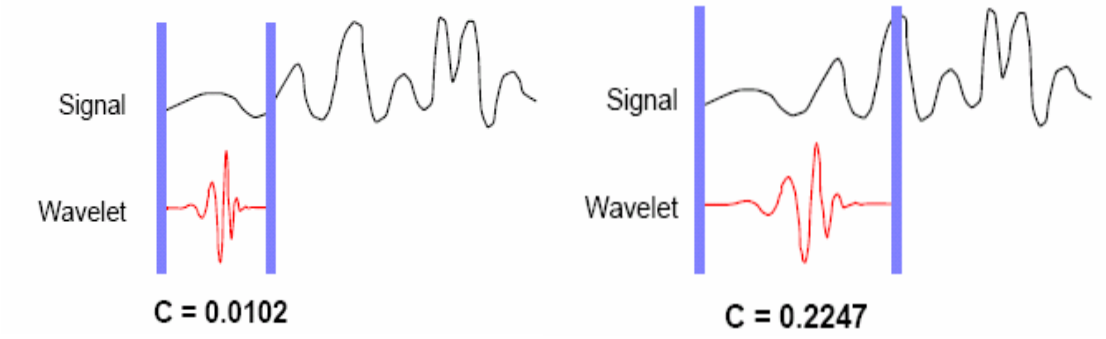

Figure 2.8 Wavelet coefficients as a function of scale and position (from Misiti et al., 2004).

After publication of Morlets work, Yves Meyer was the first to recognize the connection between Morlets wavelets and earlier mathematical wavelets (Mackenzie, 2001). Meyer discovered a new family of wavelets that are orthogonal. In 1986 Stéphane Mallat, a former student of Meyer, linked the wavelets for MRA and simplified working with wavelets greatly. Ingrid Daubechies discovered a new set of wavelets (Fig. 2.9) that were orthogonal and almost as easy to program as Haar wavelets (Mackenzie, 2001).

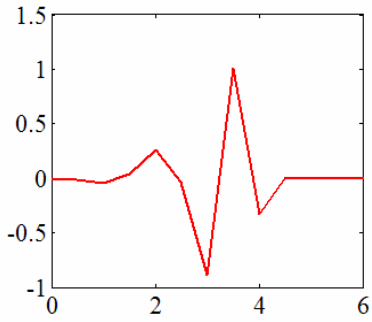

Figure 2.9 Daubechies-4 wavelet.

These important steps were critical points in the development of wavelets and were followed by a great increase in applications. Today, wavelet techniques have become a regular means for analyzing localized variations of power within a time series (Torrence and Compo, 1998) and wavelets are used in many fields of science and engineering. Applications range from data reduction for computer models to drawing of animated characters in full-length films.

2.2.2 Use of Wavelets in Reservoir Characterization

Although wavelets have been increasingly used in many disciplines of science and engineering over the past few decades, their use in the petroleum industry has been somewhat limited. Out of the thousands of papers written on the wavelet-based studies, only about a dozen papers have been presented related to petroleum industry applications (Guan et al., 2004).

One of these studies used wavelet transforms of data from northeastern Mexico to detect hydrocarbons by analyzing variations of amplitude with frequency of the seismic waves (Burnet and Castagna, 2003). The use of wavelet transforms to prospect hydrocarbon potential from seismic interpretations proved to be more efficient than results obtained from broadband analysis of seismic sections.

In a reservoir characterization study, Panda et al. (2000) showed that wavelet transforms were a reliable tool for detection of layer boundaries and discontinuities in 1-D and 2-D permeability data. Panda et al. also showed wavelets to be a good tool for denoising data and that wavelets could be used for scale-up purposes to reduce the size of the data set without losing valuable information (Fig. 2.10). This property of wavelet transforms becomes useful specifically where the reduction of large data sets is essential to minimize the computation time.

(a) Grid Size: 256x256 (b) Scaleup Grid: 16x16

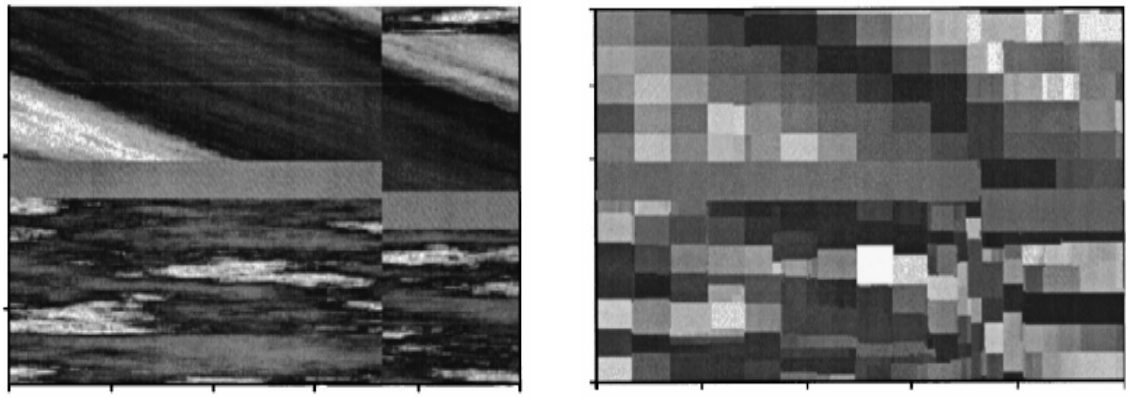

Figure 2.10 Scale-up of fine-scale 2-D permeability data using wavelet analysis (from Panda et al., 2000).

In their study, Jansen and Kelkar (1997) proposed that, due to its ability to cope with non-stationarity of the data, wavelet transformations could prove useful for capturing the transient nature of the cross correlations that are used in describing flow paths in the reservoir and defining inter well communucation. In another study for upscaling reservoir properties, Jansen and Kelkar (1998) used wavelets on 2-D and 3-D fine-scale permeability data. They were able to use this technique to preserve the important fine-scale characteristics in coarse scale models. The authors concluded that, by using wavelets, local discontinuities in the data could be preserved better than was possible using conventional methods.

Wavelet transforms can also be used for compression of data from downhole measurements up to a ratio of 15:1 without losing any significant information in the data (Bernasconi et al., 1999). This result is very important as it allows a great increase of acquisition rate for logging while drilling (LLD). Other possible uses of wavelets for analysis of LWD data along with further insight on this issue are discussed in Appendix A.

Further application of wavelet transforms can be found in well testing. Soliman et al. (2003) showed that, due to the two main characteristic properties of wavelets (smoothing of the basic signal and retention of the details), wavelets are effective tools

for interpreting pressure transient data. Using the Daubechies family of wavelets for analyzing pressure signals for four field examples, Soliman et al. were able to associate the abrupt changes in the data and sharp discontinuities with wellbore and reservoir events, whereas other reservoir events such as faults and no flow boundaries were determined by amplitude changes. The ability to identify events more quickly makes the wavelet technique an excellent candidate for comprehensive interpretation of well test data.

2.2.3 Evaluation of Well Logs Using Wavelets

Well logs are a common source of data for evaluation of subsurface sedimentary deposits. In this study we use wavelets to assess variations of grain size logs and associate these variations with the processes that occurred at the time of deposition. Similar analyses of cyclic properties of sedimentary rocks using wavelets have been conducted on well log data from the Egret Member, offshore eastern Canada (Prokoph and Agterberg, 2000), and the Ormskirk Sandstone, Irish Sea (Rivera et al., 2004).

Prokoph and Agterberg (1999) proposed that, by using wavelet analysis, accumulation rates and stratigraphic completeness could be calculated. The Morlet wavelet is suitable for detecting the cyclic components in the sedimentation, and Prokoph and Agterberg were able to detect and correlate periodic-cyclic successions of marine sediments in the Western Canada Sedimentary Basin. Cycles defined from gamma-ray logs, sonic logs, lithology, and biotic change were in good correlation. Prokoph and Agterberg believed these cyclicities were climatically controlled and mainly generated as a result of the 100 kyr Milankovitch cycles of Earth's orbital eccentricity.

Prokoph and Agterberg (2000) introduced wavelet analysis for evaluation of the quality of oil-source rock data and high-resolution stratigraphy from well log data. Prokoph and Agterberg (2000) analyzed 17 gamma-ray logs from wells penetrating the Egret Member, which is an oil-source rock succession of 55 m to 227 m thickness. This study also used the Morlet wavelet. They were able to detect the sedimentary cycles

displaying multiple periodicity, and they determined the wavelengths from visual inspections of the 2-D scaleogram plots of the wavelet coefficients. The dominant gamma-ray cycles ranged in wavelength from 2.8 m to 24 m and had ratios similar to the periodicities of Milankovitch cycles. They concluded that climatic cycles were the controlling element on the cyclic behavior of sedimentation in the Egret Member. Automatic detection of discontinuities such as unconformities and faults from the log data using wavelets was also achieved.

Prokoph and Agterberg showed that wavelet analysis of lithostratigraphic units with distinct periods could define targets for petroleum exploration from logging data. Their study contradicted previous studies in the area and is open to reinterpretation, because it was based on assumptions about the time span of sedimentary periods. Thicknesses of sedimentary sections can not be directly related to time because age resolution data generally contain large errors due to relatively large standard errors in radiometric age determination.

Rivera et al. (2004) highlighted advantages of wavelets for detection of abrupt changes compared to other signal analysis methods. They applied the wavelet transform with complex Morlet type wavelets for analyzing well log and core data for 3 zones in the Ormskirk Sandstone. They identified sedimentary features that corresponded to cyclicities identified from different petrophysical properties. The average wavelengths obtained for each of the three zones correlated with the ratios of the Milankovitch precession, obliquity, and eccentricity cycles. This supported the claims from previous studies that climate may have had a significant control during the aeolian deposition of the Ormskirk Sandstone.

On the other hand, this study did not cover analysis of the data using other signal processing methods, after comparing the signal analysis methods of FT, semivariogram analysis, and wavelets using two simple cases, one for a signal with an abrupt change in the frequency and another for a signal with two superimposed frequencies. Thus the advantage of wavelet analysis remains somewhat unclear for this specific case.

Furthermore, in their studies they did not use any sectioning other than the three zones for assessment of the reliability of the wavelengths obtained.

2.3 Milankovitch Orbital Cyclicities

The studies of Prokoph and Agterberg (2000) and Rivera et al. (2004) both linked the depositional variations to climatic effects caused by Milankovitch cycles. One goal of this study is to assess evidence for similar Milankovitch cyclic controls on depositional variations within the Chinji and the Nagri Formations.

Milankovitch orbital cycles are named after Milutin Milankovitch, a Serbian astronomer who first calculated the duration and magnitude of these variations (Niebuhr, 2005). Milankovitch cycles refer to variations in the Earth's precession, obliquity (axial tilt), and eccentricity resulting from times of increased or decreased solar radiation that directly influence the Earth's climate system and potential sea-levels. Changes in the sea level may produce repetitive variations in the stratigraphical record (Niebuhr, 2005).

Precession defines the gradual change in the direction of the Earth's axis, carving out an imaginary cone shape with a 21,000-year (19-23 kyr) average span cycle. Obliquity refers to 41,000-year cycle when the angle at which Earth's axis is tilted with respect to the plane of its orbit, varying between 22.1 degrees and 24.5 degrees. Eccentricity is the changing shape of Earth's orbit, from nearly circular to elliptical around the Sun, over an average cycle of about 100,000 years (95-136 kyr) with a peak in eccentricity which occurs around an average of 400,000 years.

CHAPTER III
ANALYSIS METHODS

3.1 Brief Description of Data Available

Data used in this study are log data of in the form of lithology, sediment grain size and calculated resistivity values for a continuous 2100 meter section of the Siwalik Group (Fig. 3.1; Willis 1993a). Measurements collected at a sampling rate (f_s) of 1 measurement/meter span in the Chinji and the Nagri Formations-and include the upper interval of the underlying Kamlial and the lower interval of the overlying Dhok Pathan formations.

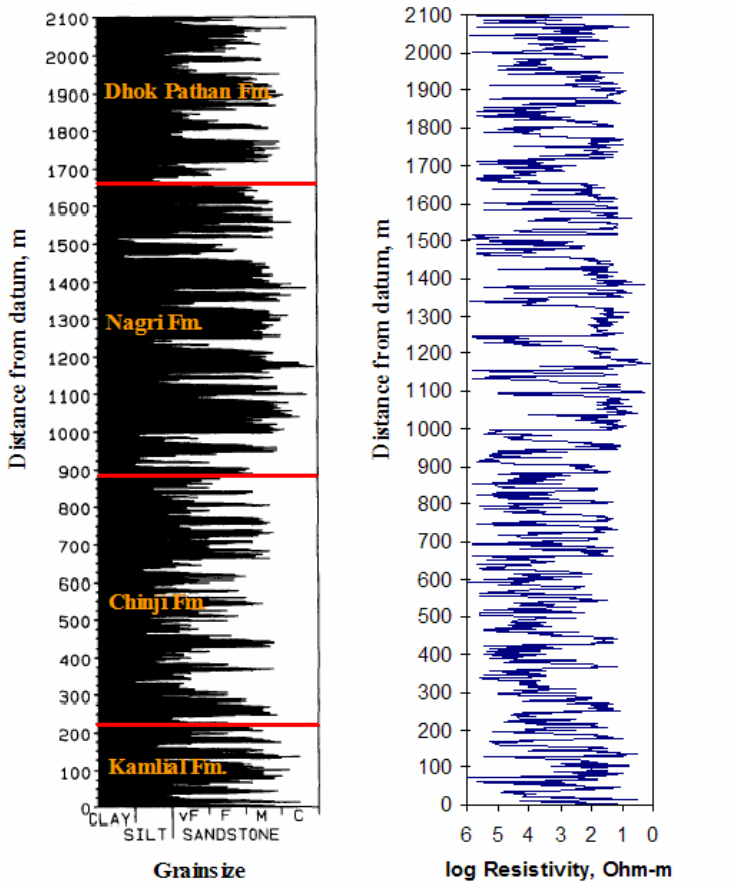

Figure 3.1 Log data of the grain sizes of sediments (from Willis, 1993a).

The vertical continuity of these data is unusual for strata from this depositional setting. The log measurements show a marked change in sedimentary characteristics at several different scales. The Chinji - Nagri boundary marks a major time of change in the Siwalik Group with increasing depositional rates and coarsening of successions. Variations in the grain size correlate well with variations in the formation and formation boundaries appear as abrupt grain size changes.

Formations within the Siwalik Group reflect changing proportions of the sandstone relative to the proportions of mudstone. The percentage of sandstone in the Chinji Formation is considerably lower than that of the Nagri Formation (Table 3.1).

Table 3.1 Characteristic values associated with the Chinji and Nagri formations (from Willis, 1993b).

	Kamlial Fm.	Chinji Fm.	Nagri Fm.	Dhok Pathan Fm.	Total
Formation Thickness (m)	220+	665	770	445+	2100
Formation Ages Ma	18.3-15.3	15.2-10.6	10.5-8.10	8.9-?	18.3-<9
Sandstone % of Log	67.1	30.0	68.7	50.4	52.0
Overbank % of Log	32.9	70.0	31.3	49.6	48.0
Mean Thickness of Storeys (m)	10.1	11.2	18.0	12.5	13.6

Other information that is used in combination with the results from wavelet analysis for assessment purposes during this study included the locations of the base and thickness of individual channel deposits, paleomagnetic ages and associated calculated accumulation rates, and overbank deposit facies interpretations.

3.2 Procedures Applied

3.2.1 Simple Statistical Measures

Data analysis studies on geological properties frequently make use of statistical methods as the simplest way to analyze the complexity of natural data. One common analysis tool

is the histogram (sample PDF) of the data. Histograms define the change of the probability of the occurrence of a particular value in the data set giving information such as recurring characteristics. A histogram is constructed by selecting a bin size and then estimating the probabilities of occurrence of the values inside subsequent bins. As a rule of thumb (Jensen et al., 2000), the bin size (Δx) is selected using

$$\Delta x = \frac{5\left(X_{\max} - X_{\min}\right)}{N} \tag{3.1}$$

where X_{max} is the largest datum, X_{min} is the minimum datum and N is the number of values in the data set.

Other important properties in statistical analysis include the arithmetic average, variance and standard deviation.

The arithmetic average ($\overline{X}$) is calculated from M samples X_1, X_2, …., X_M taken from a parent population, which has possible values X_1, X_2, …., X_I. It is an estimate of the expected value or expectation, that is, the first moment of the variable, for sets consisting of discrete variables. Thus, it is a common measure for central tendency. The variance of a random variable is its second central moment, giving information about how far from the expected value its values typically are. The standard deviation (σ), is square root of variance.

3.2.2 Wavelength Analysis

Wavelet analysis is used to identify periodic components and the evolution of these components. In this study, the wavelet analysis of resistivity values associated with grain size was performed in Matlab using the complex Morlet wavelet which actually is the product of a complex exponential wave and a Gaussian envelope defined by (Goswami and Chan, 1999, Chapter 4)

$$\psi(t) = e^{t^2/2} e^{-j5.336t} \tag{3.2}$$

where t is distance or time, and $j = \sqrt{-1}$. The wavelet coefficients are then plotted in a depth versus scale graph called a scaleogram. Scale to wavelength conversion is given by

$$\lambda = \frac{a}{f_s} \tag{3.3}$$

where λ is the wavelength (m), a is the scale, and f_s (measurement/meter) is the sampling rate.

The advantage of the Morlet wavelet for the detection of cyclic patterns and underlying frequencies over some other frequently used wavelets can be observed by looking at the simple case of a function formed of three superimposed sine functions with distinct frequencies.

$$y = \sin x + \sin \frac{x}{2} + \sin \frac{x}{3} \tag{3.4}$$

Scaleograms are generated by plotting the magnitude of wavelet coefficients, |*C*|, as a function of scale and position. The brighter points on the in these color-coded scaleograms indicate increasing similarity between the wavelet and the signal. Two different scaleograms, are generated analyzing this function for scales from 1 to 100 using the Morlet wavelet (Fig. 3.2) and the Daubechies-4 wavelet (Fig. 3.3). The 3 wavelengths of 4π, 8π and 12π for this function are easier to distinguish on the scaleogram for the Morlet wavelet. This is due to the Morlet wavelet's oscillating shape which is suitable for detecting cyclic components in the signal function.

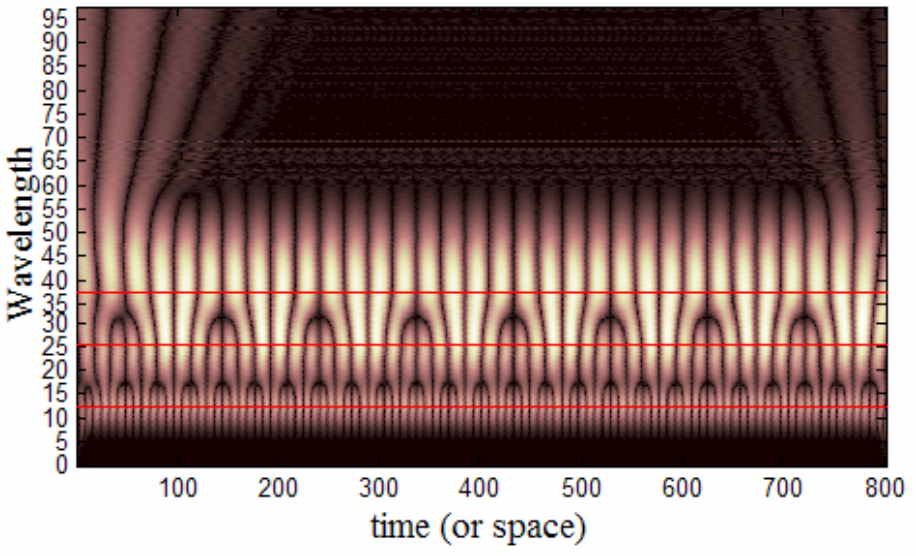

Figure 3.2 Scaleogram for simple periodic function generated with wavelet analysis using Morlet wavelet.

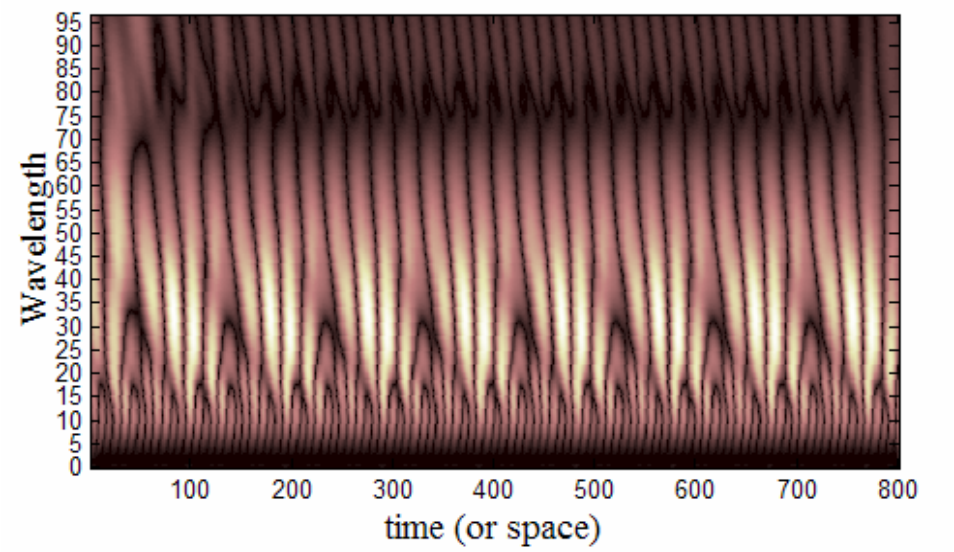

Figure 3.3 Scaleogram for simple periodic function generated with wavelet analysis using Dausbechies-4 wavelet.

Data from the Chinji and Nagri Formations were analyzed for wavelengths between 1 and 200 m. This range covers from the lower limit, set by the sampling frequency up to the largest scale cyclicities as defined by Willis (1993a), on the order of

100 m. Magnitudes of the wavelet coefficients generated from continuous wavelet transform (CWT) of the signal, which in this case is the log of grain-sizes, were plotted in a scaleogram for the Chinji and the Nagri Formations. Visual inspection of scaleograms can be useful for proposing general ideas about the behavior of the signal and the important cyclicities; however this requires prior knowledge of certain levels which is not desirable for an automated process.

To evaluate the most important cyclic components for each formation, normalized averages of the amplitudes were calculated over each depth. The average of the amplitudes ($\overline{C}$) for the whole interval for a wavelength was defined to be proportional with the sum of the amplitudes of individual scale and positions.

$$\overline{C}(a,t_B,t_T) = [\frac{1}{t_T - t_B}\int_{t_B}^{t_T} C(a,t)dt] / \left\{\max_{1\le a\le 200}\int_{t_B}^{t_T} C(a,t)dt\right\} x100 \qquad (3.5)$$

where a is the scale and t_T and t_B are the positions of the formation top and bottom, respectively.

Each formation was also divided into 5 sections with each section having top t_i and bottom t_{i+1}, where i = 0, 1, …, 4, $t_0 = t_B$, $t_5 = t_T$, and $t_{i+1} = t_i + (t_T - t_B)/5$. We were limited to five sections because the resolution of each section has to capture the 100m stacks defined by Willis (1993a). The average for each section, $\overline{C}(a, t_{i+1}, t_i)$ was also calculated to compare with $\overline{C}(a, t_B, t_T)$. In order to assess the reliability of the results and analyze the sensitivity a similar analysis was also performed using a 6 section division case, which was the maximum sectioning allowing the desired 100m resolution for assessment of large scale cyclicities and a 4 section division case, where same length of sectioning with the 5 section case was used with half sections length omitted from the top and the bottom of both formations giving shifted versions of them.

$$\overline{C}(a,t_{B+\Delta t},t_{T+\Delta t}) = [\frac{1}{t_T - t_B}\int_{t_B+\Delta t}^{t_T+\Delta t} C(a,t)dt] / \left\{\max_{1\le a\le 200}\int_{t_B+\Delta t}^{t_T+\Delta t} C(a,t)dt\right\} x100 \qquad (3.6)$$

where Δt = the length of the omitted section.

Plots of wavelength versus $\overline{C}$ (Fig. 3.4) were used to define the important cyclicities for the entire sections and the 5 sub-sections in each of the formations.

Wavelengths were selected through mathematical detection of the points that had higher amplitudes compared to its neighboring points. Three important cyclic parameters resulting in peaks on the plots were observed in each formation, which were represented by λ_0, λ_1, and λ_2 respectively. For cases where were 4 peaks, 3 of the peaks that appeared more significant were selected as wavelengths through visual inspection. The resulting plots for both the 6 section division case and the 4 section division case also had three important cyclicities. Furthermore the amplitudes of these cyclicities (wavelengths) were in good agreement with the 5 section division case.

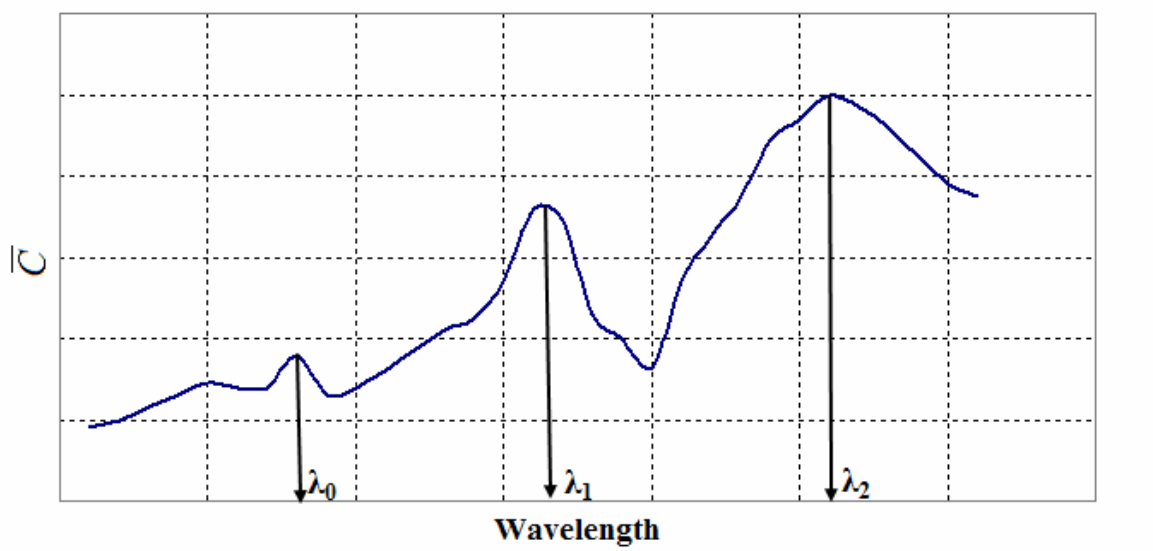

Figure 3.4 Schematic diagram illustrating how the dominant wavelength values were obtained.

To evaluate the observed wavelengths, *t*-test analyses were performed. *t*-test analysis shows how much the means of two groups are statistically different from each other. Thus, it requires a treatment group and a comparison group. Important characteristic values of the formations detailed from previous geological analysis were used for comparison purposes. The formula for the *t*-test is,

$$t = \frac{\overline{X}_T - \overline{X}_C}{\sqrt{\frac{var_T}{n_T} - \frac{var_C}{n_C}}} \tag{3.7}$$

where, $\overline{X}$ represents the arithmetic average, *var* is the variance, n is number of elements, and *T* and *C* represents the treatment and control groups respectively. The *t*-test results in a ratio indicating similarity when *t* is close to zero.

After evaluation of the amplitudes and the meanings of the wavelengths, the ratios of these dominant wavelengths were also investigated for additional information. These ratios were examined using the depositional interpretation of different scales of strata from the Willis study (1993a) as a source of comparison.

3.2.3 Boundary Analysis

Due to their low cost compared to the whole operation and their ability to provide information on a large scale, wireline logs probably comprise the most abundant source of data available for reservoir characterization. Well logs utilize indirect measurements of properties of rock properties (such as lithology) based on assessments of physical properties of the rock. Rock properties in turn, are used for purposes such as reservoir monitoring, formation evaluation, and geosteering.

A common application using well logs in the petroleum industry is the estimation of the formation boundary locations. Multiple well correlations are based on these interpretations, generally through visual analysis. However, definitions of formation boundaries based on visual analyses are not completely reliable and interpretations of two individuals of the formation boundaries using the same well log response may be different. This presents a problem as much of the work done to optimize the field performance is based on the models that are generated using such boundary interpretations. Distinguishing boundaries from well log data using an automated method would be a critical time-saving function and such a process may reduce identification errors. Formations with different characteristics should appear to be distinct using

wavelets, and thus, it may be possible to separate these formations using these techniques on overall well log responses.

An advantage of using wavelets for detection of abrupt changes and transitions is that the information generated is not restricted by the type of data the data are considered only to be a generic signal. Therefore although their response levels may be different, any type of data that is sensitive to formation characteristics could be used in a similar analysis using wavelets. To distinguish the formation boundaries, the sum of all the coefficients over scales from 1 to 200 for each depth (1-2100 m) was calculated. At any given depth t, the total coefficient for all scales was;

$$C_{tot}(t) = \int_1^{200} C(a,t)da \tag{3.8}$$

Calculated values were then plotted in a depth series and compared with resistivity log and sand percentage values for defining the locations of formation boundaries.

3.2.4 Milankovitch Analysis

For assessment of the data set for climatic controls on deposition, two separate approaches were investigated. The first approach was to use wavelength ratios, λ_1/λ_0 and λ_2/λ_0, obtained from the study and compare them with the Milankovitch cycle ratios (21:41:100) in a statistical solution. The second method was an evaluation based on comparison of depositional thicknesses of Milankovitch cycles that were generated using accumulation rates, to the profile of the energies generated by wavelet analysis around those neighborhoods.

When compared, the smallest wavelength λ_0 and the ratios λ_1/λ_0 and λ_2/λ_0 did not correlate well with the Milankovitch ratios. However, the time spans of Milankovitch ratios is a generalization with an associated variability. Thus, in most sample sets, it is not possible to estimate these values exactly. Furthermore, the data to be analyzed should be considered as samples of the population, not the population itself.

We generated a set of 500 random wavelength values λ_0, λ_1, and λ_2 for both the Chinji and the Nagri Formations based on the arithmetic average and standard deviation values of the wavelengths calculated from the analysis. In our case, the arithmetic average of λ_0 for 5 sections of the formations was;

$$\bar{\lambda}_0 = \frac{1}{5}\sum_{m=1}^{5} \lambda_{0m} \tag{3.9}$$

where, m=1,2,..,5 represents the subsequent sections for the formation considered and λ_{0m} is the λ_0 for the mth section. The standard deviation of λ_0 for 5 sections of the formations was;

$$\sigma_{\lambda_0} = \sqrt{\frac{\sum_{m=1}^{5} (\lambda_{0m} - \bar{\lambda}_0)^2}{5}} \tag{3.10}$$

where, m=1,2,..,5 represents the subsequent sections for the formation considered. The unit of standard deviation is meters since as the wavelengths we considered are in meters.

Arithmetic averages and standard deviations for wavelengths λ_1 and λ_2 were calculated similarly. Results were used for creating a sample population of 500 values for λ_0, λ_1, and λ_2 for both the Chinji and the Nagri Formations. Ratios λ_1/λ_0 and λ_2/λ_0 calculated for these values were then plotted and analyzed for Milankovitch ratios (21:41:100) with a selected 20% confidence interval.

In the analytical approach, a backwards calculation of associated channel thicknesses was used based on Milankovitch cycle periods. The sectioning was determined from Willis's studies (Fig. 3.5).

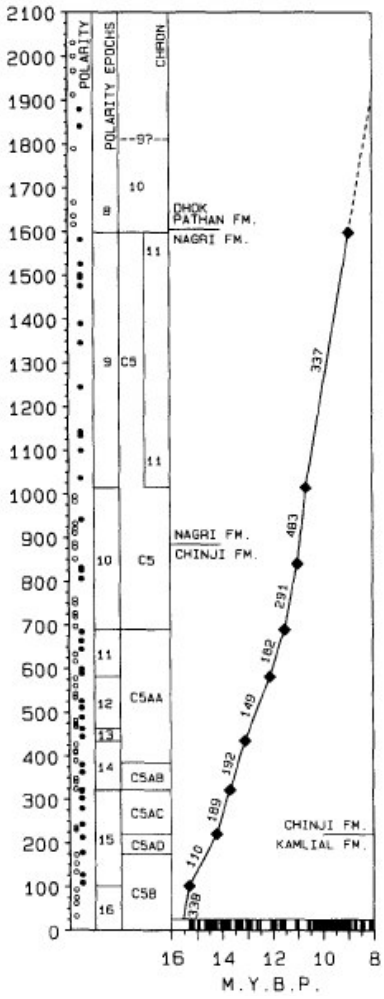

Figure 3.5 Time versus strata thickness based on magnetic polarity data (from Willis, 1993b).

The accumulation rates are given in meters/millions of years in this figure. Channel thicknesses were calculated using different accumulation rates over these sections:

$$h_{cycle} = \frac{acc_k \; x \; t_{cycle}}{1000} \tag{3.11}$$

where h_{cycle} denotes the thickness that would be observed for k^{th} interval with accumulation rate acc_k (meters/myrs) for the time span of t_{cycle} (kyrs). This approach introduces some uncertainty as accumulation rates are assumed to be constant over the

defined sections. During depositional processes accumulation rates change frequently, thus these depositional rates provide average information for these sections rather than exact information.

The associated Milankovitch thicknesses were considered as wavelengths and the total of the wavelet coefficients at positions around $\pm\Delta h$ neighborhoods of calculated Milankovitch cycle thicknesses (Fig. 3.6) were determined using

$$C_{tot}^{cycle}(i) = \sum_{k=1}^{7} \int_{t_{Bk}}^{t_{Tk}} C(a_k, t)dt \tag{3.12}$$

where i denotes the position of the scale line with k sections at scales a_k and t_{Tk} and t_{Tb} represent the top and the bottom boundaries for the k^{th} section respectively. Resulting total energies were then plotted at neighborhoods of the scale-line based on the corresponding cycle and associated Δh values.

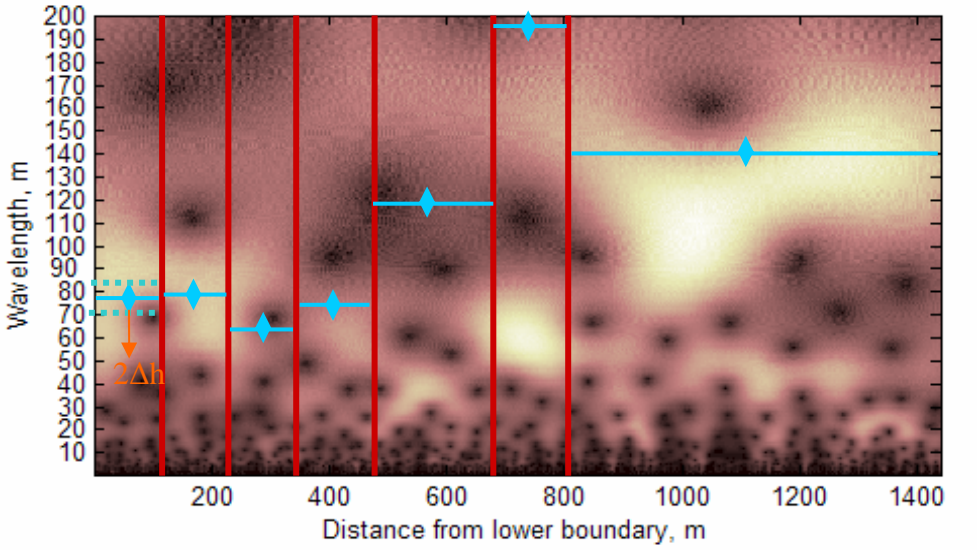

Figure 3.6 Description of scale line of calculated Milankovitch cycle thicknesses and its neighborhood for Milankovitch cycle of 413 kyr.

3.2.5 Fourier Analysis

Fourier transforms have probably been the most commonly used method in spectral analyses. They are used in many fields of science including such as physics and statistics. The Fourier transform is an integral that expresses a function using the sine and cosine functions as the basis functions. This allows the user to determine the frequencies in the data and their amplitudes by decomposing the signal. FT results are generally presented as a power spectrum plot that gives the signal's power (energy per unit time) falling within given frequency bins.

In order to search for any possible additional information within the data and also for comparing the results with wavelengths obtained from the wavelet analysis, the data set was also processed using the Fast Fourier Transform (FFT). FFT is a faster version of the Discrete Fourier Transform, giving the same discrete frequency domain representation of the data. The basic idea behind the FFT is to reduce the computation time required for a data set of N points from $2N^2$ down to $2N\log_2 N$ by changing a transform of length N into two transforms of length $N/2$. The FFT generates absolute value and phase components, both of which carry important information. However there is no systematic method to interpret phase information; therefore we used only the magnitudes for analysis purposes. Considering the period extending from f=0 to f_s where f_s is the sampling frequency, an even symmetry is observed around the center point, called the Nyquist frequency, resulting in repetition of the information because of aliasing.

CHAPTER IV
RESULTS

4.1 Simple Statistical Measures

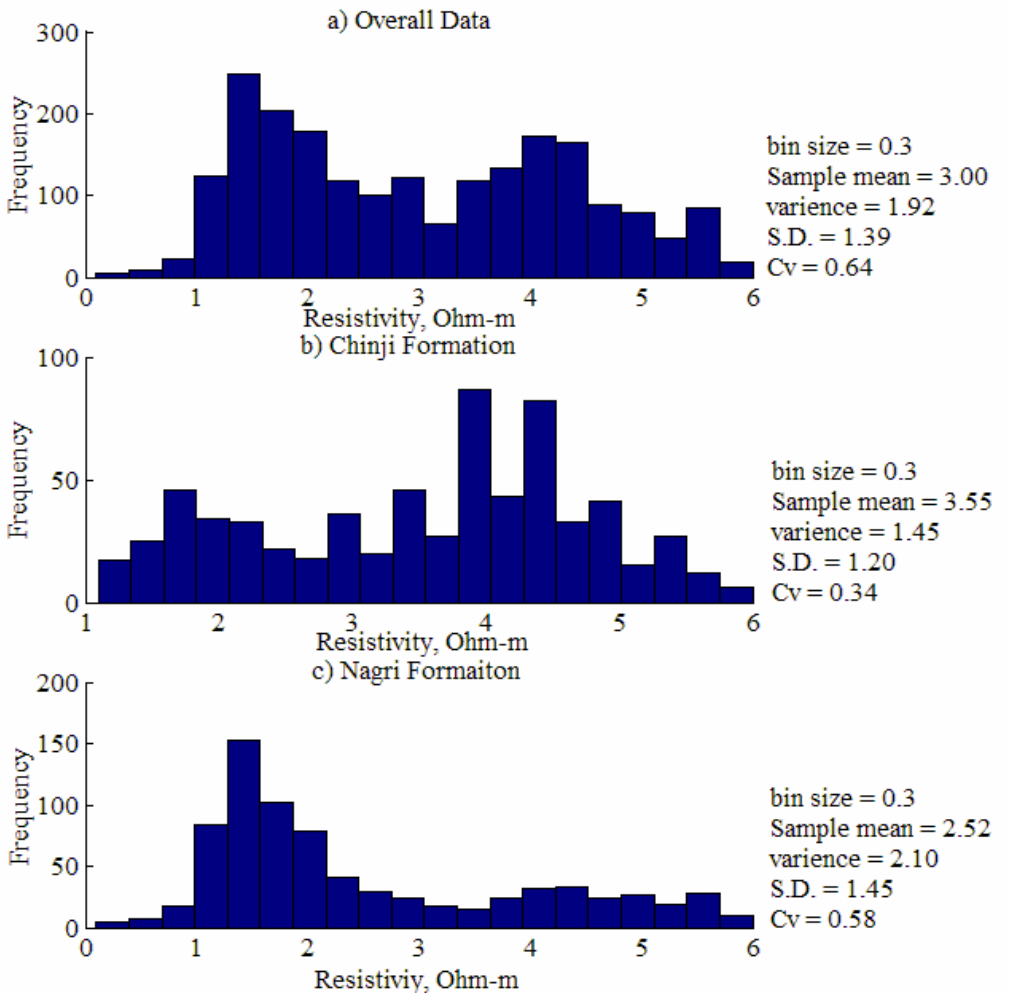

Figure 4.1 Sample PDF (Histogram) representations for the resistivity data.

Due to the large number of data considered, the minimum increment in the data (0.1) was a limiting factor as it was larger than the bin size calculated using Eq. 3.1 and was a

limiting property. 0.3 was chosen as the bin size for this study for smoothing purposes. The histogram was used to define the modes of the resistivity profile. The histogram representation of the resistivity profile overall data set and for the Chinji and Nagri Formations for a bin size of 0.3 along with the important statistical properties are as seen in Fig. 4.1. Two different modes are observed on the histogram generated for the overall data set representing the sand deposits and the overbank deposits.

The inverse proportional relationship between grain size and resistivity is also suggested in the histograms for the formations. The resistivity values for the Chinji Formation, with higher overbank content, are higher compared to the Nagri Formation with higher sand content. The probability plot of the data is as shown in Fig. 4.2. Two different slopes that are related to sands and overbanks are observed.

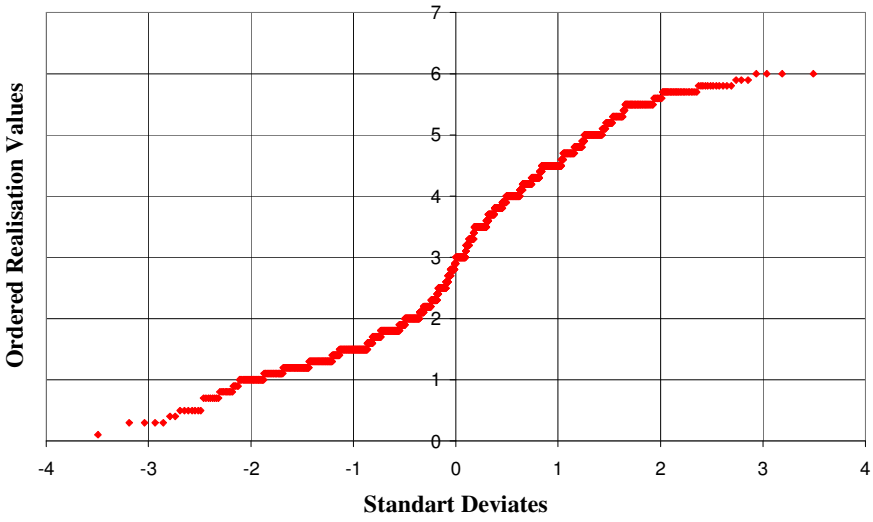

Figure 4.2 Probability plot for the data.

4.2 Wavelengths

Scaleograms are generated by plotting the magnitude of wavelet coefficients, $|C|$, as a function of scale and position. Brighter points on these color-coded scaleograms indicate increasing similarity between the wavelet and the signal. Scaleograms generated for the

Chinji Formation (between 216m-885m) and the Nagri Formation (between 886m-1654m) are in Figure 4.3. There is a large amplitude cyclic component of 100 to 120 m wavelength in the Nagri Formation taking place at the section between 1130m-1360m of the signal.

(a) Chinji formation

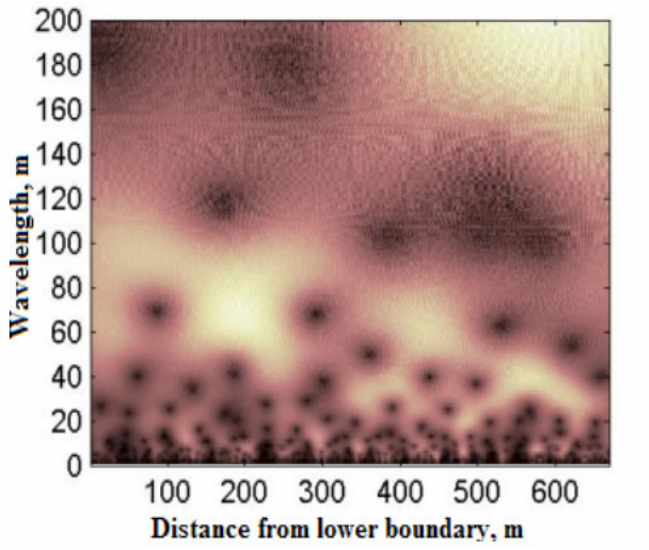

(b) Nagri Formation

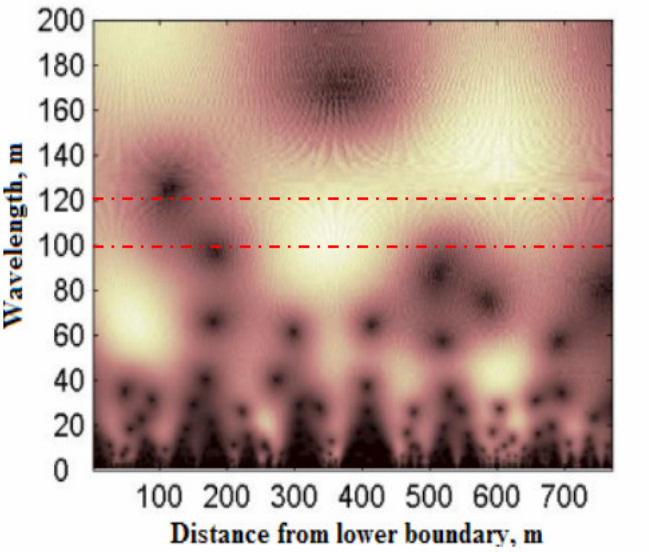

Figure 4.3 Wavelet scaleograms for Chinji and Nagri Formations, dark=low amplitude and white=high amplitude.

Plots of $\overline{C}(a, t_B, t_T)$ and $\overline{C}(a, t_{i+1}, t_i)$, $i = 0, 1, \ldots, 4$, versus a for the Chinji and Nagri Formations (Figs. 4.4 and 4.5) show three important cyclic components for the formations. [the bold blue lines represent the overall formations and the colored lines represent the relevant sections of the formations] The three important scales of cyclicities observed for the entire sections and the 5 sub-sections in each of the formations are listed in Table 4.1.

Table 4.1 The three dominant wavelengths for Chinji and Nagri Formations and their 5 subsections.

Meters	Formation/Section	λ_0 (m)	λ_1 (m)	λ_2 (m)
216-885	Chinji	10	35	83
216 – 351	Chinji 0	20	58	92
352 – 484	Chinji 1	9	23	68
485 – 617	Chinji 2	9	35	83
618 – 750	Chinji 3	7	30	53
751 – 885	Chinji 4	6	34	80
886-1654	Nagri	22	49	132
886 – 1038	Nagri 0	22	67	200
1039 – 1191	Nagri 1	22	53	121
1192 – 1344	Nagri 2	24	50	110
1345 – 1497	Nagri 3	22	44	136
1498 – 1654	Nagri 4	21	46	136

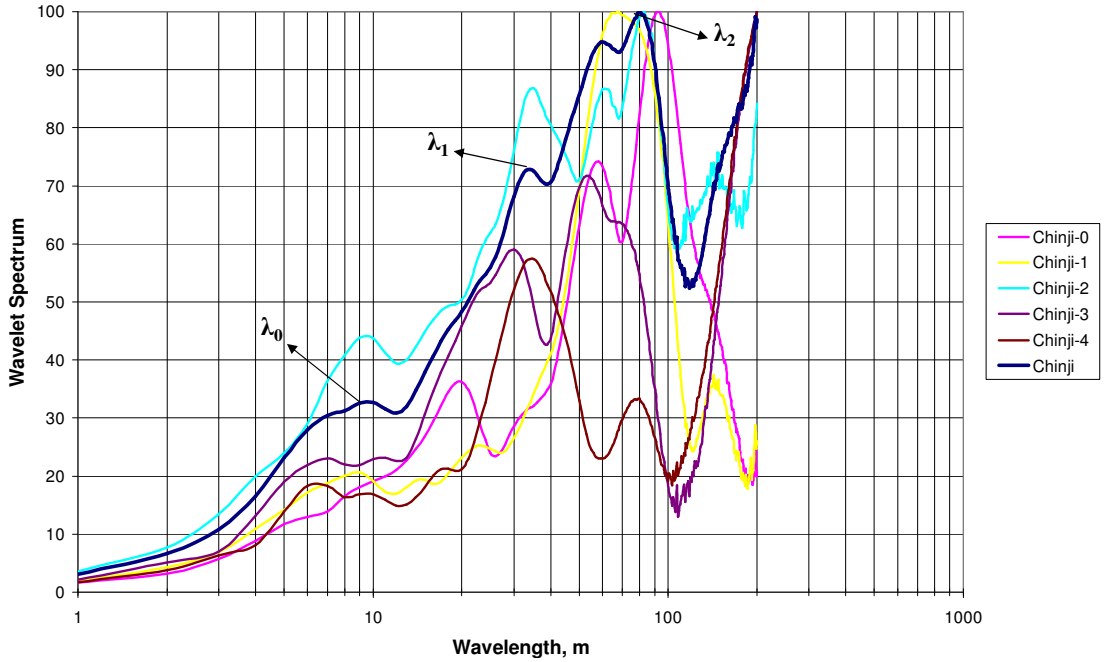

Figure 4.4 Wavelet spectra for the Chinji Formation, using the whole formation (blue bold) and the divided 5 sections.

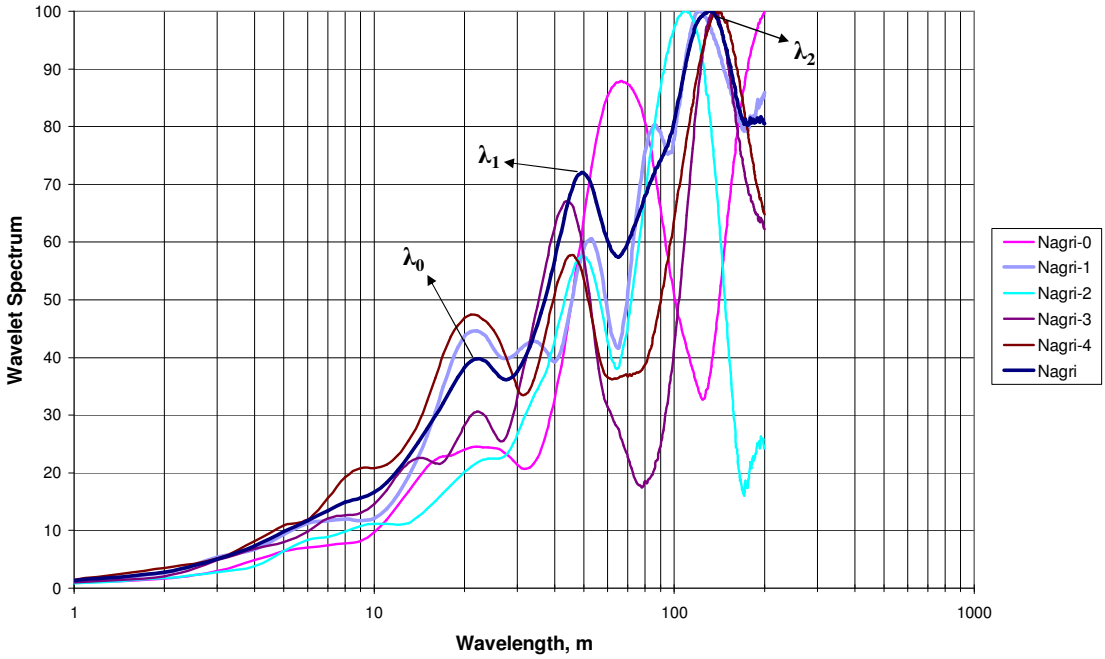

Figure 4.5 Wavelet spectra for the Nagri Formation, using the whole formation (blue bold) and the divided 5 sections.

To further assess the reliability of the λ's derived from Figs. 4.4 and 4.5, $\overline{C}(a, t_{i+1}, t_i)$, i = 0, 1, …, 5 (i.e., six sections) were calculated. The amplitude of the peaks differed from the 5 section case, but the location of the peaks denoting the wavelengths were relatively similar with the 5 section case (Fig. 4.6 and Table 4.2). The resulting values λ_0 and λ_1 for this case agreed within 6.3% with the 5 section case for the Nagri Formation. The largest difference was for λ_2 with 11.3%. However, this may be caused by the change in the interval length has the greatest effect on calculation of the largest wavelength. The results for Chinji Formation for six section case had higher variability in wavelengths with up to 26.2%. This is a result of Chinji covering a shorter section compared to Nagri which makes it harder to investigate using six sections.

Furthermore, using the jacknife, λ values were also calculated for the formations using 4 sections (Table 4.2). This was performed by using a similar division criterion with the 5 section analysis and by analyzing the 4 sections after omitting half a section's length from each formation's upper and lower boundary (Fig. 3.1). For the Nagri Formation, once again, the highest variability was observed for λ_2 with 20.7% however, values λ_0 and λ_1 for this case agreed well with the 5 section cas. The comparison of wavelengths for the Nagri Formation using 5 section division and 4 section division after exclusion of end data is shown in Fig. 4.7.

Table 4.2 Average wavelengths for Nagri Formation using 4, 5, and 6 sections.

Formation/Separation	λ_0 average (m)	λ_1 average (m)	λ_2 average (m)
Nagri 5 Sections	22.2	52.0	140.6
Nagri 6 Sections	20.8	51.0	124.7
% difference	6.3	1.9	11.3
Nagri 4 Sections	22.0	49.5	111.5
% difference	0.9	4.8	20.7

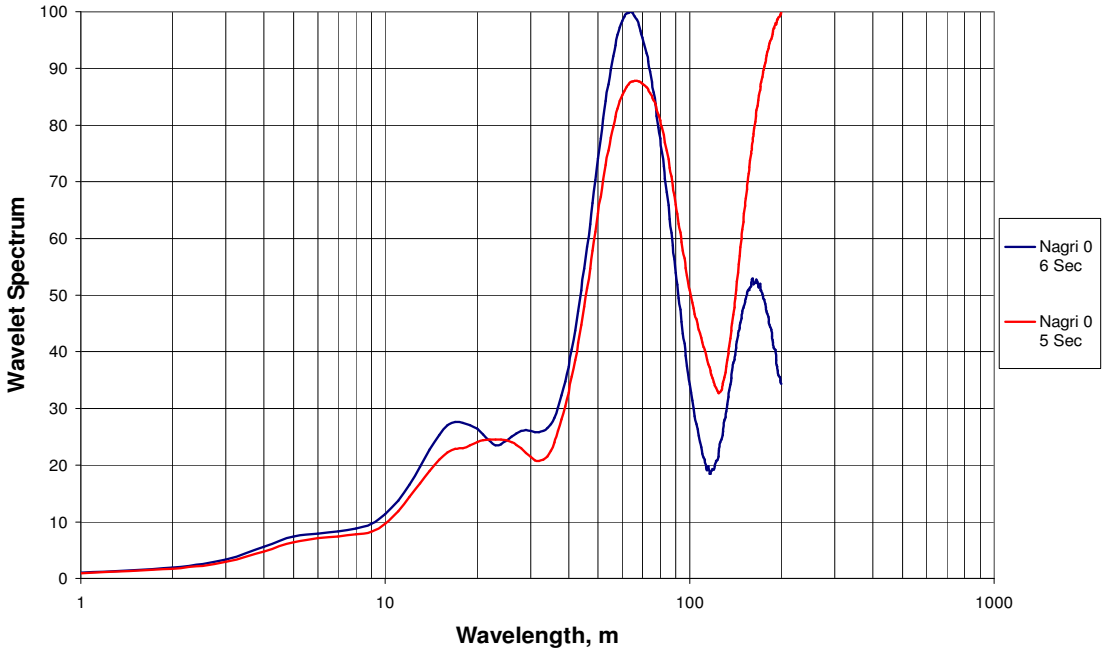

Figure 4.6 Nagri Formation wavelet spectra comparison for the first section of 6 sections and the first section of 5 section divisions.

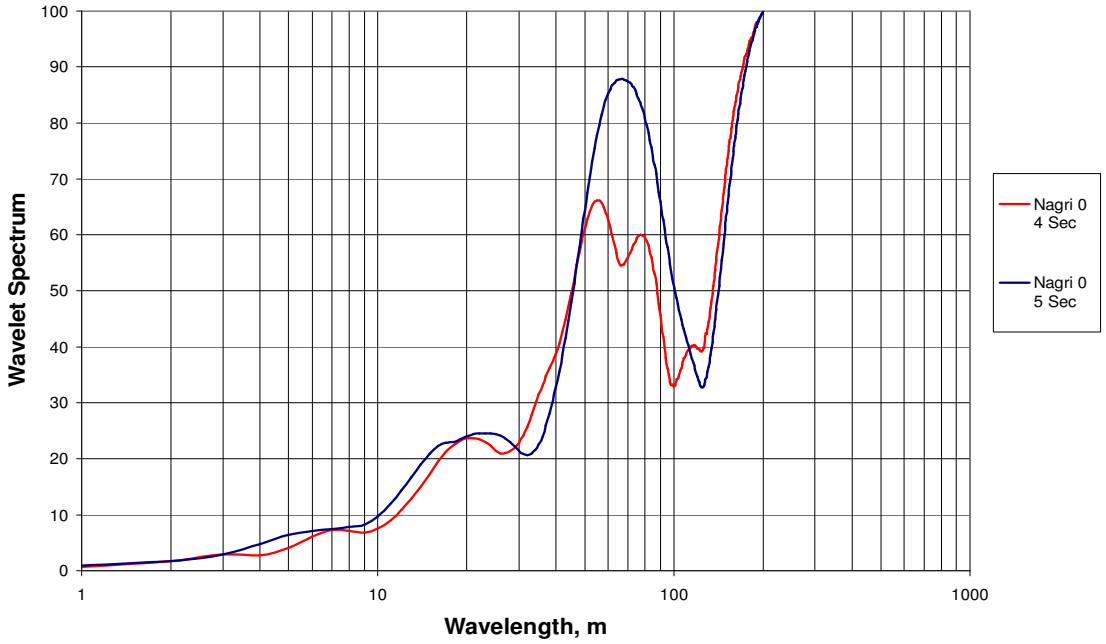

Figure 4.7 Nagri Formation wavelet spectra comparison for the first section of 4 sections excluding the formation ends and the first section of 5 section divisions.

In order to define the relationships of the λ's with sedimentary features, *t*-tests were performed on the λ values in conjunction with important characteristics previously identified by Willis (1993) (Table 4.3). For the Chinji Formation, the average of the smallest of these wavelengths, λ_0 (10.2m) was observed to be within the range of thicknesses of the channel sizes; 5 to 15m defined by Willis. However, there is an observed difference between the Nagri formation λ_0 (22.2m) and the average channel thicknesses defined by Willis for the Nagri Formation.

Table 4.3 *t* values for λ_0's and thickness of channels for Chinji and Nagri Formations.

Formation	Average Wavelength (m)	Thickness of Channels (m)	*t* value
Chinji	10.2	11.2	-0.38
Nagri	22.2	18.0	3.64

The difference shown in Table 4.3 for the Nagri Formation may be explained by channel amalgamation. Siwalik group is a fluvial system where deposition is controlled by channels. In such systems, a channel may be deposited and incise another, previously deposited channel depending on several other factors such as the discharge rates and span area of the river. Deposition during the Chinji was controlled by a comparably small river system with lower discharge rates, thus, the adjacent channels were generally separated from each other. As the larger river system with higher discharge rates took control during the deposition of Nagri however, channel stacking is more common. Compared to Chinji Formation, where the sand bodies are generally isolated channels, sand bodies in the Nagri Formation are in most cases comprised of stacks of multiple rivers that incise each other. Thus, the λ_0's for the Chinji and Nagri represent different geological events.

The main reason for this discrepancy between the meanings of λ_0's is understood to be the inability of the wavelet analysis to distinguish individual channels in the stacks from the log data for the Nagri Formation data. Thus the wavelet analysis considers instead of multiple channels forming a stack, there is a continuous section of sand over

such intervals. The λ_0 observed in the Nagri Formation agrees with average thicknesses of all the sand units calculated from the data, including both the isolated channels and the stacks supports this observation (Table 4.4).

Table 4.4 *t* value for λ_0 and thickness of sand units for the Nagri Formation.

Formation	Average Wavelength (m)	Thickness of Sand Units (m)	*t* value
Nagri	22.2	25.7	-0.83

Previous studies by Willis (1993a, b) of the Chinji and Nagri Formations indicate that the major sandstone bodies were not randomly distributed within the cross section. They showed a trend, with clusters of vertically interconnected sands with scales of about 100 m thicknesses, separated by overbank deposits with fewer isolated sandstone bodies. The largest of the wavelengths, λ_2, were in good agreement for both Chinji and Nagri with this depositional trend of stacked, vertically clustered sediments (Table 4.1).

The intermediate wavelength, λ_1, was determined to correspond to the average separation distance between the bases of channels for the Chinji and the average separation distance between the bases of the sand units for the Nagri (Table 4.5).

Table 4.5 *t* value for λ_1 and separation distance between bases of channels for the Chinji Formation and t value for λ_1 and separation distance between the bases of the sand units for the Nagri Formation.

Formation	Average Wavelength (m)	Separation of bases of Channels (m)	*t* value
Chinji	36.0	36.7	-0.08
Formation	Average Wavelength (m)	Separation of bases of Sand Units (m)	*t* value
Nagri	52.0	45.3	0.85

The transition at the Chinji-Nagri boundary is marked by an increased coarsening in the alluvial succession and changes in the wavelengths. There is a large change in the channel thicknesses as seen in λ's after the Chinji-Nagri boundary. This difference of channel thicknesses up to 2 to 3 times corresponds well with the suggested change in the river systems defined during sedimentologic analysis.

Using λ_0 as a measure of sand body thickness, we calculated the ratios λ_1/λ_0 and λ_2/λ_0 to represent dimensionless wavelengths of the larger scale cyclicities for the 5 section division case. Resulting values for the overall formations and the representative sections are listed in Table 4.6.

Table 4.6 Dimensionless wavelengths λ_1/λ_0, λ_2/λ_0, and λ_2/λ_1 for overall formations and the 5 sections.

Meters	Formation/Section	λ_1/λ_0	λ_2/λ_0	λ_2/λ_1
216-885	Chinji	3.5	8.3	2.4
216 – 351	Chinji 1	2.9	4.6	1.6
352 – 484	Chinji 2	2.6	7.6	3.0
485 – 617	Chinji 3	3.9	9.2	2.4
618 – 750	Chinji 4	4.3	7.6	1.8
751 – 885	Chinji 5	5.7	13.3	2.4
886-1654	Nagri	2.2	6.0	2.7
886 – 1038	Nagri 1	4.4	13.4	3.0
1039 – 1191	Nagri 2	2.4	5.5	2.3
1192 – 1344	Nagri 3	2.1	4.6	2.2
1345 – 1497	Nagri 4	2.0	6.2	3.1
1498 – 1654	Nagri 5	2.2	6.5	3.0

Comparison of the ratios of λ's to the percentage of sandstones (Fig. 4.8) shows that, as the percentage of sandstones increase the values of λ_1/λ_0 (R_1) and λ_2/λ_0 (R_2) stay relatively similar which may suggest similar controlling factors on deposition. There is a sudden jump in magnitudes of λ_2/λ_0 and λ_1/λ_0 ratios at the boundary which reflects the time of larger river system with higher discharge taking over control at the Chinji – Nagri boundary.

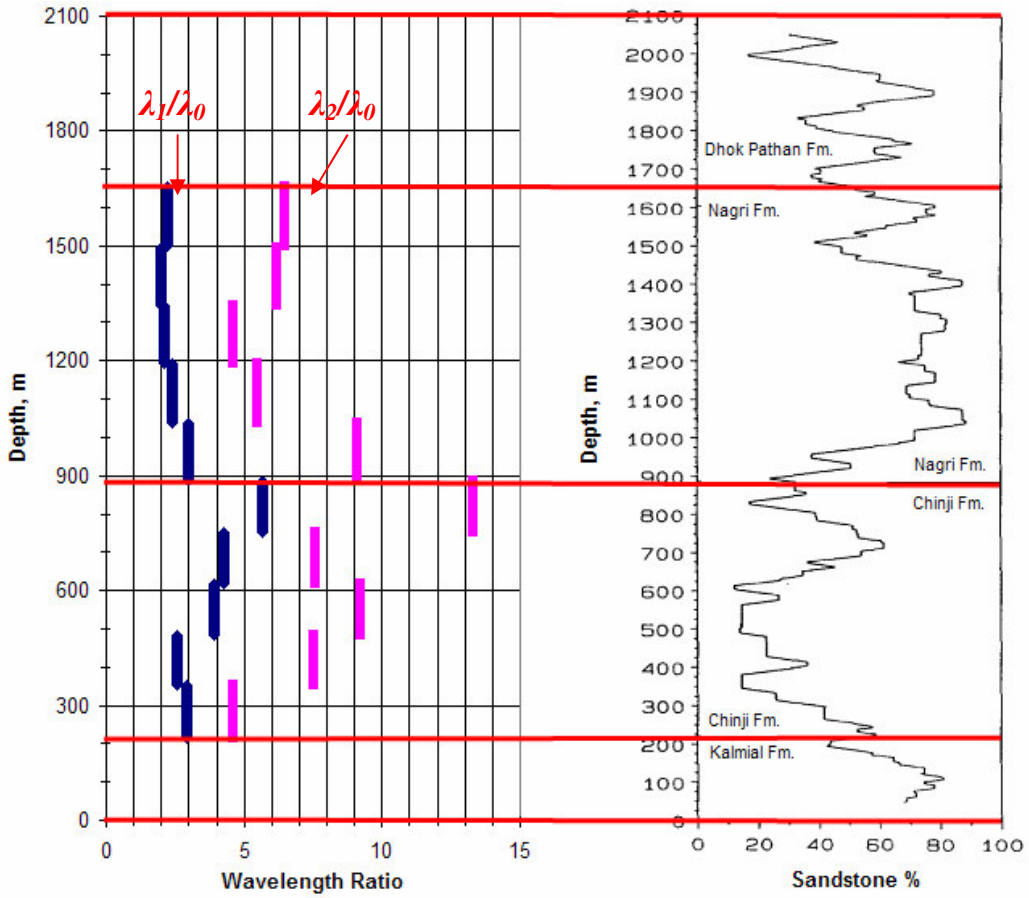

Figure 4.8 Comparison of dimensionless wavelengths to the percentage of sandstone, the blue lines defining λ_1/λ_0 and the pink lines defining the λ_2/λ_0 values for successive sections.

4.3 Analysis of Formation Boundaries

In order to compare with the sediment profile, C_{tot} for all scales at each depth was plotted in a depth series (Fig. 4.9). The variation in the resulting graph had good correlation with resistivity profile and sand percentage values. The total wavelet energies were related to the sand proportions of the formations. There were distinctly different characteristic trends for each formation, suggesting changes in these periods. Furthermore, both the Chinji section and the Nagri section of the generated profile had upward increasing total values which are in good correspondence with general behavior of upward coarsening deposits.

In the Chinji Formation, the cyclicities are shorter with a general upward-increasing trend in the total energy. This may be attributed to increasing cyclicirt as Nagri times approach. The behavior shows a dramatic change in the Chinji-Nagri Formation boundary, where afterwards, during the Nagri period, the cycles are much longer in scale and much more apparent.

Separation of formation boundaries based on Figure 4.9 could be easier to a trained eye as it represents a clearer image of the changes compared to the resistivity values. Also, by assigning threshold levels to data, sections may be determined using an automated manner. The advantage of using such a method in conjunction with conventional log analysis techniques is that this method is not limited to the type of data used. Thus, as long as there is a data set that is represented in a time or depth series on the formation, results from this method could be used in distinguishing different formations that have different responses at the measurement phase.

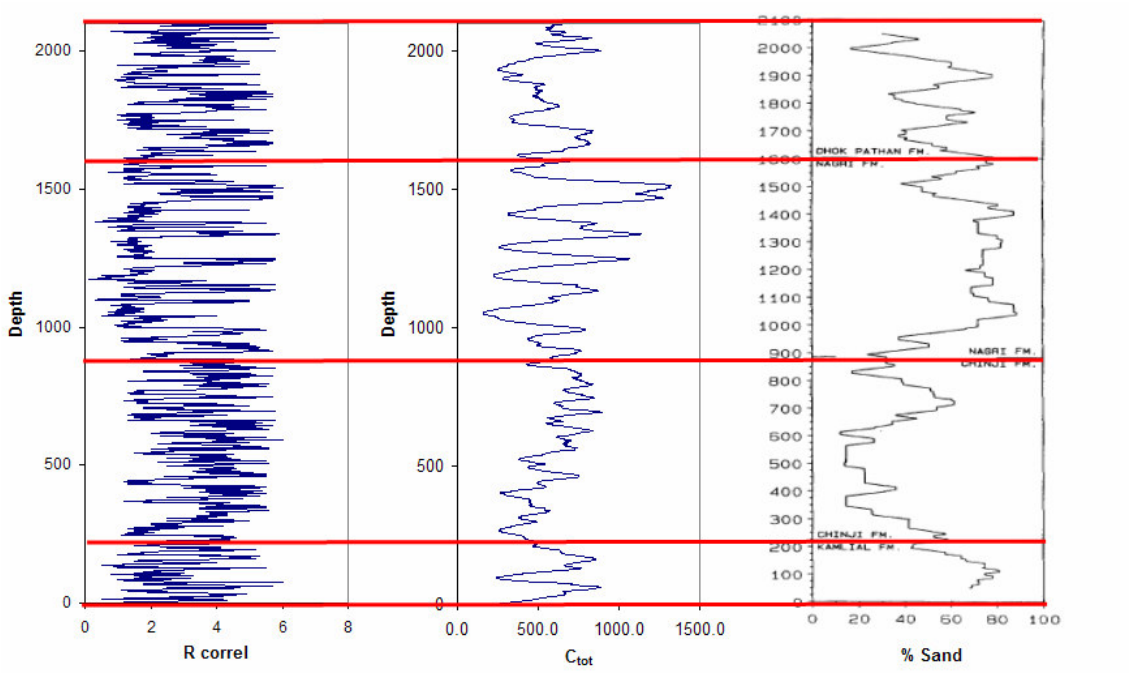

Figure 4.9 Comparison of total wavelet energies vs depth with resistivity correlation and the sand percentages.

4.4 Milankovitch Analysis

Assessments of Milankovitch cycle ratios (21:41:100) were carried out using a statistical approach based on R_1 and R_2 obtained from the study and an analytical approach based on accumulation rates. Calculated R_1 (λ_1/λ_0) and R_2 (λ_2/λ_0) ratios based on the 500 random values of λ_0, λ_1 and λ_2 were plotted for the Chinji Formation (Fig 4.10) and the Nagri Formation (Fig 4.11). The bold lines in these graphs represent the exact Milankovitch cycle ratios of 41:21 and 100:21 respectively. The boxes with the transparent green background define the limits of the 20% confidence interval. For the Chinji (Fig. 4.10), out of the 500 values of (R_1, R_2) only 5.8% of them fell into the box denoting the confidence region. The Nagri (Fig. 4.11) had 14.2% of the values out of the 500 falling in the confidence region.

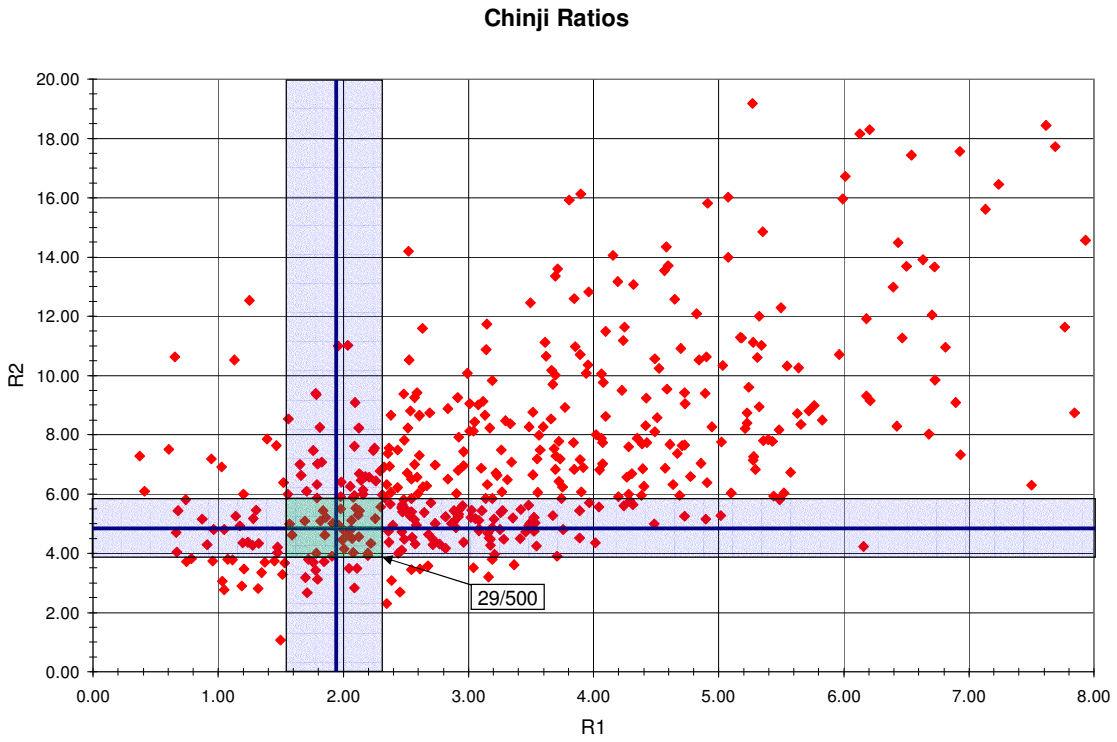

Figure 4.10 R_1 (λ_1/λ_0) versus R_2 (λ_2/λ_0) plot for the Chinji Formation.

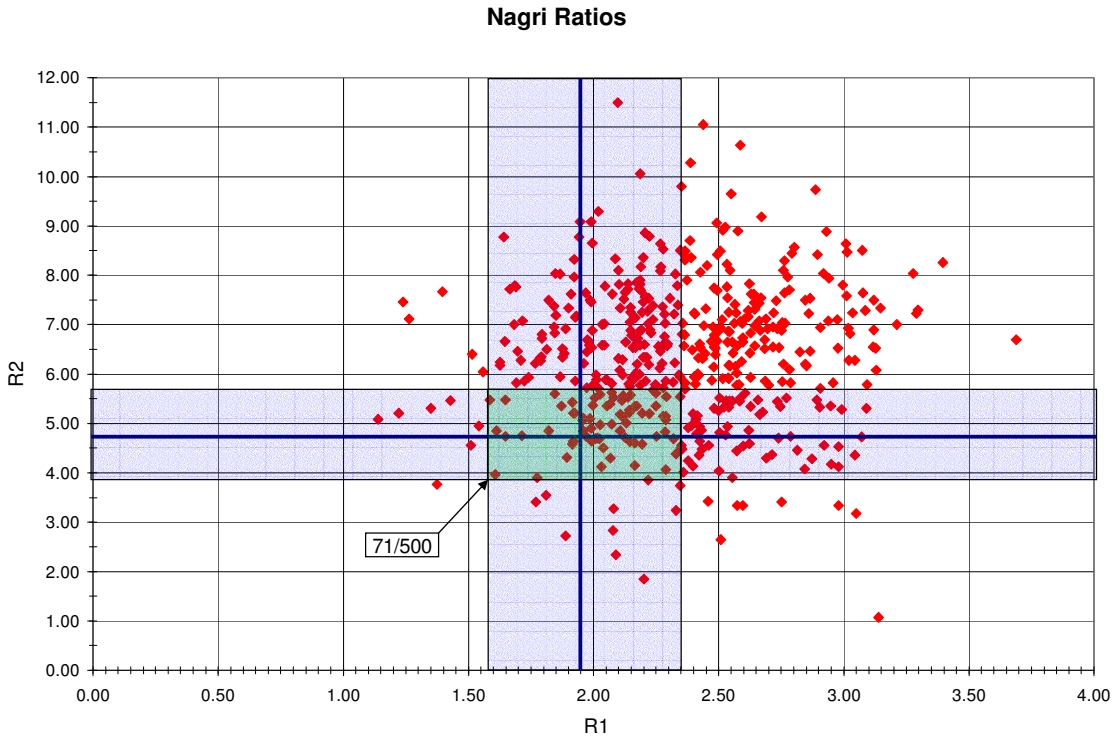

Figure 4.11 R_1 (λ_1/λ_0) versus R_2 (λ_2/λ_0) plot for the Nagri Formation.

It might be argued that the larger probability for the Nagri Formation might suggest a slightly higher climatic influence on deposition. However, even for this case, the probability is small (less then 15%). From these results, it cannot be argued that there was a strong climatic control during deposition for either of the formations.

Seven sections of different depositional rates defined from Willis's work for the Chinji and the Nagri Formation and their corresponding accumulation rates (meters/my) are as seen in Table 4.7.

Calculated thicknesses of depositional sections corresponding to these rates, using the Milankovitch cycles and their associated time intervals commonly referenced in the literature for each cycle period are shown in Table 4.8.

Table 4.7 Accumulation rates over sections defined from Willis data.

Metes	Section	meters/my
216-320	Chinji 1	189
321-430	Chinji 2	192
431-580	Chinji 3	149
581-690	Chinji 4	182
691-840	Chinji 5	291
840-1020	C6-N1	483
1021-1654	Nagri 2	337

Table 4.8 Average Milankovitch cycle accumulations (m) for sections based on accumulation rate data and associated Δh sections.

Cycle	Years	Ch1	Ch2	Ch3	Ch4	Ch5	Ch6-Ng1	Ng2	Δh
1	19000	3.6	3.6	2.8	3.5	5.5	9.2	6.4	±0.5
1	23000	4.3	4.4	3.4	4.2	6.7	11.1	7.8	±0.5
2	41000	7.7	7.9	6.1	7.5	11.9	19.8	13.8	±1.0
3	95000	18.0	18.2	14.2	17.3	27.6	45.9	32.0	±2.5
3	136000	25.7	26.1	20.3	24.8	39.6	65.7	45.8	±2.5
3	413000	78.1	79.3	61.5	75.2	120.2	199.5	139.2	±5.0

A plot of total energy at neighborhoods of the scale line for the Milankovitch 2 cycle of 41 kyrs with a ±1.0 m neighborhood (Fig. 4.12) shows an increasing profile and for the Milankovitch 3 cycle of 413 kyrs with a ±5.0 m neighborhood (Fig. 4.13) shows a decreasing profile as the scale line is moved upwards. The intersection at 0 of x-axis represents the positioning of the scale line at the 41 kyrs and at 413 kyrs thicknesses of depositional sections respectively. It would be safe to assume this point to show a peak in total energies in case of climatic controls on deposition. However the total energy at this point also falls in the increasing and decreasing profiles. The total energy diagrams at corresponding neighborhoods for the other cycles are presented in Appendix B.

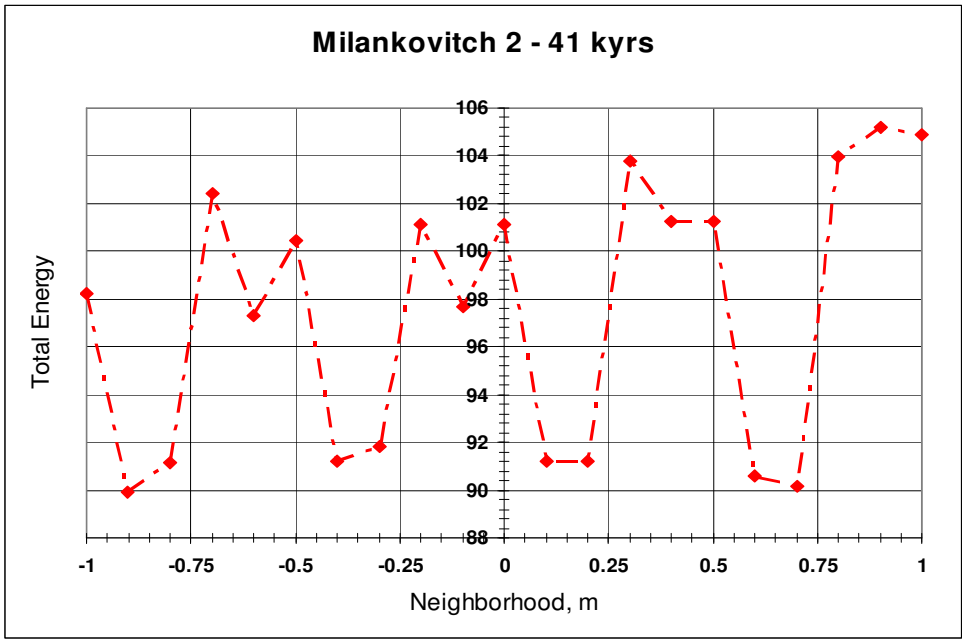

Figure 4.12 Total energy diagram around ±1.0 m neighborhood of 41 kyr Milankovitch 2 depositional cycle thickness associated with the depositional rates.

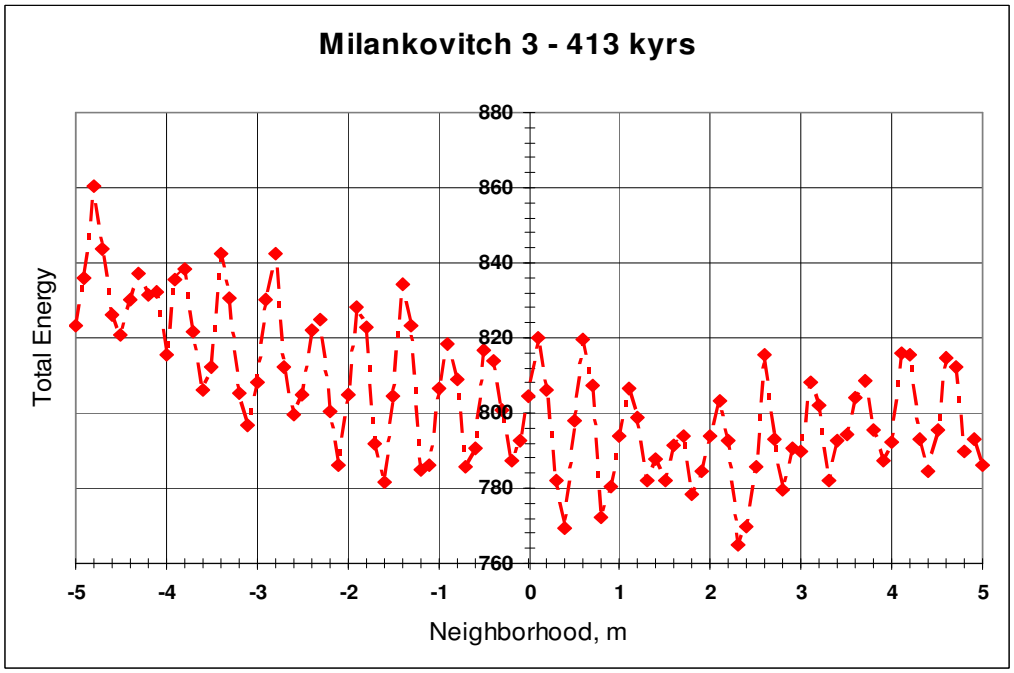

Figure 4.13 Total energy diagram around ±5.0 m neighborhood of 413 kyr Milankovitch 3 depositional cycle thickness associated with the depositional rates.

Thus, results from both the statistical and the analytical approaches indicated that climatic controls were not the major driving mechanism of deposition for the Chinji and the Nagri Formations.

4.5 Fourier Analysis

The generated log-log scale plots of frequency versus power spectrum for the Chinji Formation (Fig. 4.14) and the Nagri Formation (Fig. 4.15) both have a slope of near -1. This corresponds closely with the so called fingerprint of the critical systems, the flicker noise where the power spectrum scales as 1/f at low frequencies. In these types of systems, there is an interaction between the elements of the system which cannot be understood just by studying the individual constituents in isolation (Bak et al., 1988). Most natural systems such as flow of rivers are of this type.

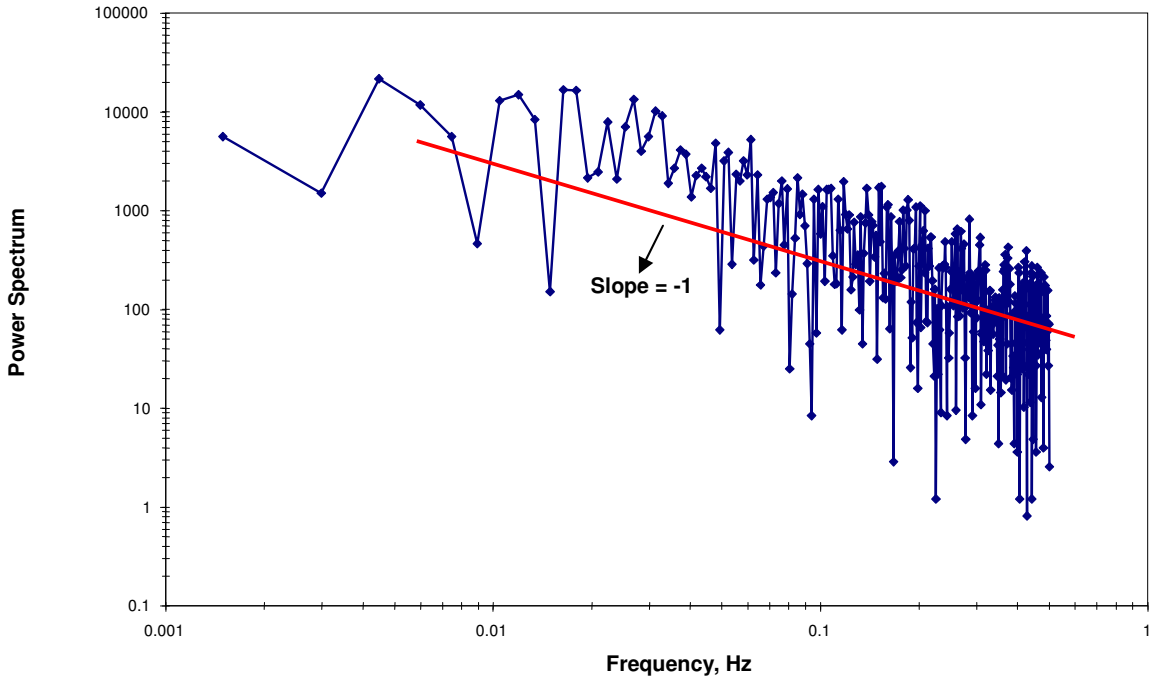

Figure 4.14 Power spectrum for Chinji formation with Fourier analysis.

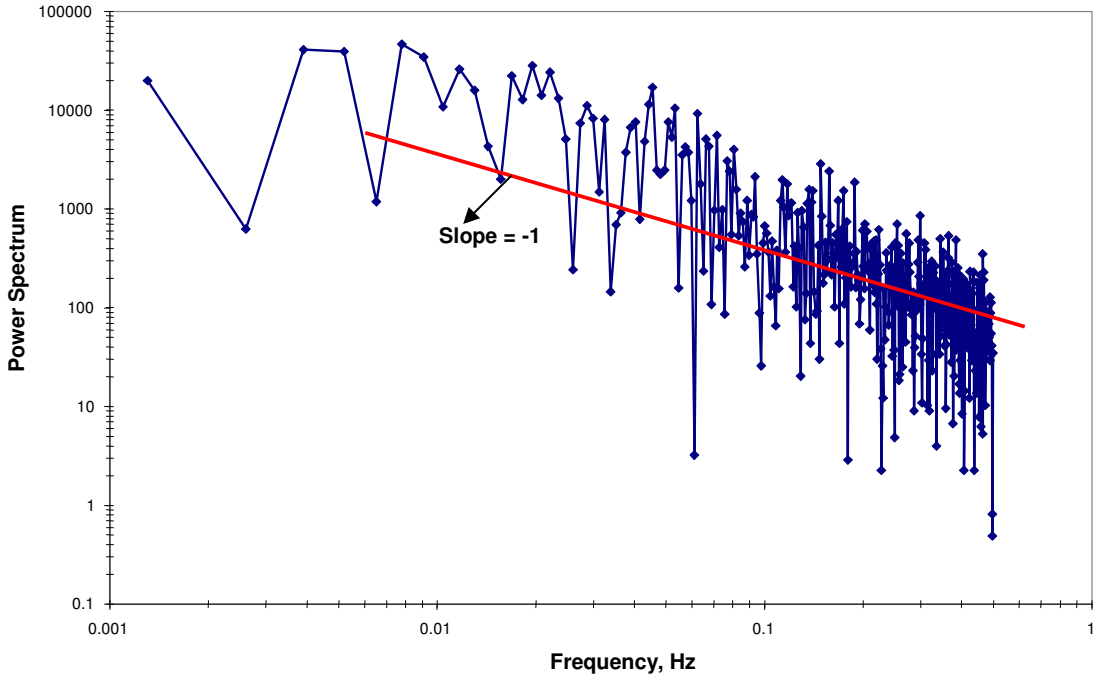

Figure 4.15 Power spectrum for Nagri formation with Fourier analysis.

A linear presentation of the power spectra (Figs. 4.16 and 4.17) clearly indicate the small wavelength cyclicities that were previously defined both in the studies of Willis and the analysis using wavelets. Furthermore, the Fourier analysis was able to define the cyclicities yet it was unable to define the locations. The higher wavelength cyclicities identified using wavelet analyses, on the other hand, were not large in the Fourier analysis spectra.

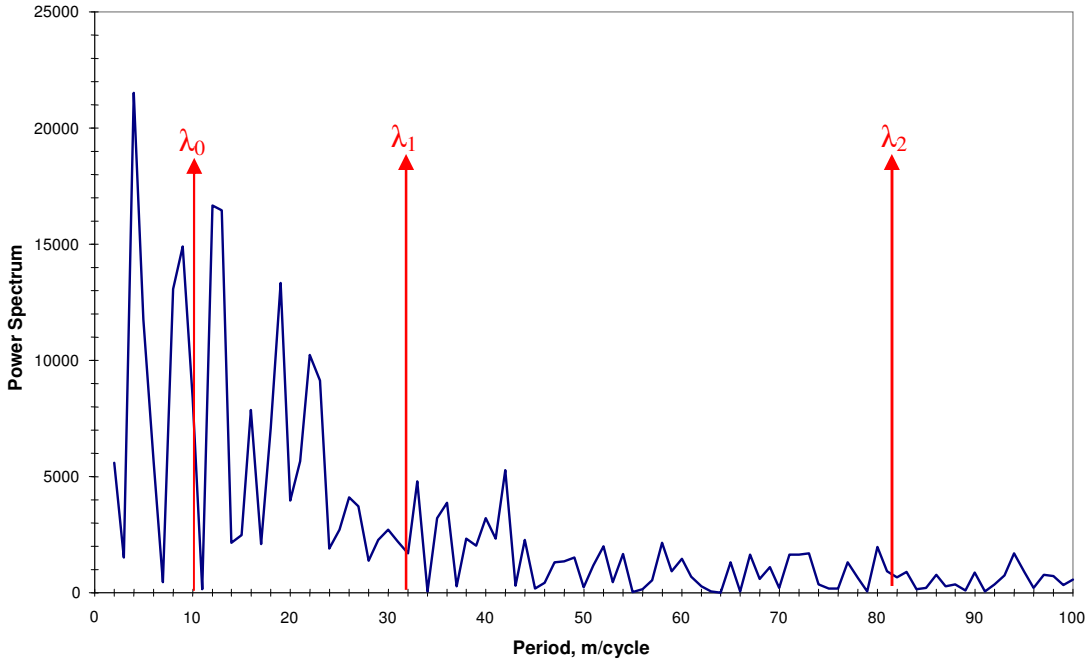

Figure 4.16 Linear presentation of the power spectra for the Chinji formation.

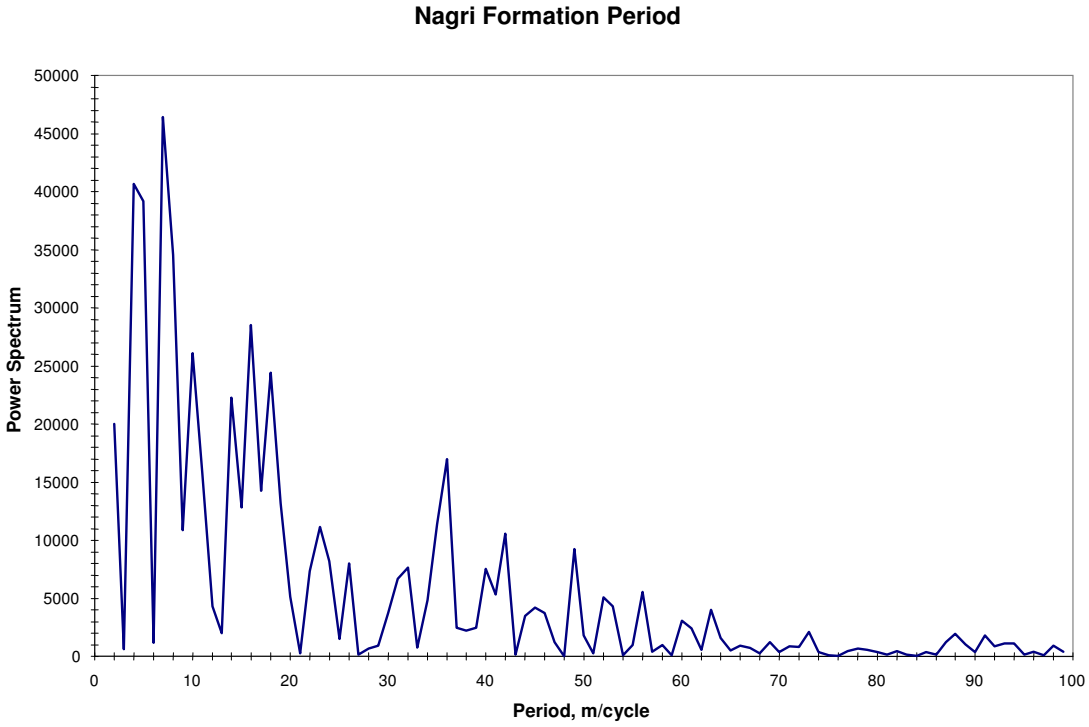

Figure 4.17 Linear presentation of the power spectra for the Nagri formation.

CHAPTER V
RECOMMENDATIONS FOR FUTURE WORK

The data that was used in this study were previous measurements of grain sizes and associated resistivity values for a section of 2100 m. However this 2100 m of continuous data represents measurements along several sections. Thus it does not represent a perfectly vertical stratigraphic section. Additional information about depositional characteristics of the Chinji and Nagri Formations may be revealed if such perfectly vertical succession is to be analyzed in the future.

Several other areas begun in this investigation could be pursued, including

1) The geological significance of the weak or non-existent influence of Milankovitch frequencies could be assessed;

2) The analysis here has been based on only one variable; more variables (eg well log measurements) may often be available and the analysis needs to be extended to allow for multivariate wavelet methods;

3) The ratio R_1 appeared to be constant through the Chinji and Nagri analysis and we inferred that this was because of the similar depositional processes in the two formations. This needs to be tested in other settings.

4) C_{tot} appears to be a useful characteristic for boundary detection but needs to be tested further before being proposed as a reliable boundary detection method.

CHAPTER VI
SUMMARY AND CONCLUSIONS

This study showed that wavelet analysis is a very powerful multi resolution analysis tool which can be used for definition of important cyclic parameters of data sets of non stationary signals that can be represented in a time series.

Fluvial deposits are notoriously difficult to correlate in the subsurface, because definition of lithic trends is complicated by superimposed scale of variation. Wavelet analysis identified major scales of vertical sandbody variation within a thick fluvial succession, based on previous detailed sedimentologic studies to reflect vertical trends within river channels, avulsion of channels across aggrading floodplains, and a larger-scale clustering of channel bodies that may reflect an allocyclic process. Reliability of the wavelengths was assessed by dividing the formations into subsections, the resulting wavelength for the sections were in good agreement with the wavelengths of the overall formations. Changes of these three depositional scales across formations that were previously interpreted to reflect displacement of a smaller river system by a larger system were also defined.

Our results suggest that wavelet analysis can define important stratigraphic breaks and internal periodic patterns within fluvial deposits. This study indicates that continued refinement of wavelet analysis and interpretations may lead to automated methods to define similar scales of stratigraphic variation to aid correlations of subsurface deposits.

Assessment of Milankovitch cyclicities within these formations using both the statistical and the analytical approaches indicated that climatic effects of predicted frequencies were not the major driving mechanism of cyclic deposition. However the wavelet analysis proved to be a useful approach in quantification of the qualitative properties of these formations and thus made it possible to draw conclusions about climatic effects on deposition from the data using mathematical methods.

Moreover, in analysis of the data that is not strictly cyclic in nature, wavelet analysis is more efficient compared to the Fourier analysis. Fourier analysis was able to

identify the smaller scales of cyclicities but not locations of cycle boundaries. Wavelet analysis on the other hand can be used to identify both the cyclicities and their locations.

NOMENCLATURE

N	North
FT	Fourier Transform
MRA	Multi Resolution Analysis
CWT	Continuous Wavelet Transform
C	Wavelet Coefficient
FFT	Fast Fourier Transform
R_1	Ratio 1
R_2	Ratio 2
kyrs	1000 years
M.Y.B.P.	Million years before present

REFERENCES

Aniekwena, A.U., McVay, D.A., Ahr, W.M., and Watkins, J.S., 2003, Integrated characterization of the thin-bedded 8 Reservoir, Green Canyon 18, Gulf of Mexico, SPE 84051, *in* SPE 78th Annual Technical Conference and Exhibition Proceedings: Society of Petroleum Engineers.

Bak, P., Tang, C., and Wiesenfeld, K., 1988, Self-organized criticality: *Physical Review*, vol. A38, p. 364.

Bernasconi, G., Rampa, V., Abramo, F., and Bertelli. L., 1999, Compression of downhole data, SPE/IADC 52806, *in* SPE/IADC Drilling Conference Proceedings: Society of Petroleum Engineers/International Association of Drilling Contractors.

Boggess, A., and Narcowich, F.J., 2001, *A First Course in Wavelets with Fourier Analysis*, Prentice-Hall, New Jersey, p 155.

Burnett, M., and Castagna, J., 2003, Application of spectral decomposition to gas basins in Mexico: *The Leading Edge*, p. 1130-1134.

Goswami, J. and Chan, A.K., 1999, *Fundamentals of Wavelets*, John Wiley, New York.

Guan, L., Du, Y., and Li, L., 2004, Wavelets in petroleum industry: Past, present and future, SPE 89952, *in* SPE 79th Annual Technical Conference and Exhibition Proceedings: Society of Petroleum Engineers.

Jansen, F.E., and Kelkar, M.G., 1997, Upscaling of reservoir properties using wavelets, SPE 38876, *in* SPE 72nd Annual Technical Conference and Exhibition Proceedings: Society of Petroleum Engineers.

Jansen, F.E., and Kelkar, M.G., 1998, Upscaling of reservoir properties using wavelets, SPE 39495, *in* SPE India Oil and Gas Conference and Exhibition Proceedings: Society of Petroleum Engineers.

Jensen, J.L., Lake, L.W., Corbett P.W., and Goggin D.J, 2000, *Statistics for Petroleum Engineers and Geoscientists*, Elsevier, Amsterdam, p 338.

Kumar, R., Ghosh, K.S., and Sangode, S.J., 2003, Mio-Pliocene sedimentation history in the northwestern part of the Himalayan Foreland Basin, India: *Current Science*, vol. 84, no. 8, p. 1006-1013.

Loughlin, P.J., Pitton, J.W., and Atlas, L.E., 1992, Proper time-frequency energy distributions and the Heisenberg uncertainty principle, *in* IEEE-SP International Symposium Proceedings: Institute of Electrical and Electronics Engineers-Signal Processing Society , p. 151-154.

Mackenzie, D., 2001, Wavelets: seeing the forest–and the trees: *Beyond Discovery*, December, p. 1-8.

Misiti, M., Misiti, Y., Oppenheim, and Poggi, J.M., 2004, Wavelet Toolbox User Guide. Available from World Wide Web:http://www.mathworks.com/access/helpdesk/help/pdf_doc/wavelet/wavelet_ug.pdf.

Morlet, J., Arens, G., Fourgeau, E., and Giard, D., 1982a, Wave propagation and sampling theory-part I: Complex signal and scattering in multilayered media: *Geophysics*, vol.47, no. 2, p. 203-221.

Morlet, J., Arens, G., Fourgeau, E., and Giard, D., 1982b, Wave propagation and sampling theory-part II: Sampling theory and complex waves: *Geophysics*, vol.47, no. 2, p. 222-236.

Niebuhr, B., 2005, Geochemistry and time-series analyses of orbitally forced Upper Cretaceous marl-limestone rhythmites (Lehrte West Syncline, northern Germany): *Geological Magazine*, vol. 142, p. 31-55.

Panda, M.N., Mosher, C.C., and Chopra, A.K., 2000, Application of wavelet transforms to reservoir-data analysis and scaling: *SPE Journal*, vol. 5, no. 1, p. 92-101, also paper SPE 60845.

Prokoph, A. and Agterberg, F.P., 1999, Detection of sedimentary cyclicity and stratigraphic completeness by wavelet analysis: An application to Late Albian cyclostratigraphy of the Western Canada Sedimentary Basin: *Journal of Sedimentary Research*, vol. 69, July, p. 862-875.

Prokoph, A., and Agterberg, F.P., 2000, Wavelet analysis of well-logging data from oil source rock, Erget Member, offshore eastern Canada: *AAPG Bulletin*, vol. 84, no. 10, p. 1617-1632.

Rivera, N.A., Ray, N., Jensen, J.L., Chan, A.K., and Ayers, W.B., 2004, Detection of cyclic patterns using wavelets: An example study in the Ormskirk Sandstone, Irish Sea: *Mathematical Geology*, vol. 36, no. 5, p. 529-543.

Soliman, M.Y., Ansah, J., Stephenson, S., and Mandal, B., 2003, Application of wavelet transform to analysis of pressure-transient data: *SPEREE*, vol. 6, no. 2, p. 89-99, also paper SPE 83670.

Torrence, C., and Compo, G.P., 1998, A practical guide to wavelet analysis: *Bulletin of the American Meteorological Society*, vol. 79, no. 1, p. 61-78.

Willis, B. J., 1993a, Ancient river systems in the Himalayan foredeep basin, Chinji Village Area, northern Pakistan: *Sedimentary Geology*, vol. 88, p. 1-76.

Willis, B. J., 1993b, Evolution of Miocene fluvial systems in the Himalayan Foredeep through a two kilometer-thick succession in northern Pakistan: *Sedimentary Geology*, vol. 88, p.77-121.

Willis, B.J., and Behrensmeyer, A.K., 1994, Architecture of Miocene overbank deposits in northern Pakistan: *Journal of Sedimentary Research*, vol. B64, no. 1, p. 60-67.

Willis, B.J., and Behrensmeyer, A.K., 1995, Fluvial systems in the Siwalik Miocene and Wyoming Paleogene: *Palaeogeography, Palaeoclimatology, Palaeoecology*, vol. 115, p. 13-25.

APPENDIX A

POSSIBLE USES OF WAVELETS IN REAL TIME DRILLING DATA ANALYSIS

Measurement While Drilling and Logging While Drilling

Measurement while drilling (MWD) and logging while drilling (LWD) has become an increasingly popular area in petroleum engineering over the past two decades. Data collected downhole during a drilling operation such as torque in bit (TOB), weight on bit (WOB), bending moment, accelerations, RPM, and temperature are included in MWD whereas LWD defines the measurements of formation properties that are taken during drilling in a similar fashion to open hole wireline logging with the exception that the tools are integrated to the bottom hole assembly and the data is collected as the drilling operations are uninterrupted.

Although these real time data acquisition methods may increase the operational costs and introduce additional risks to the operations, they are still valuable especially in cases where it is almost impossible to gather formation measurements using conventional wireline tools such as in the case of highly deviated wells. Furthermore, MWD and LWD have become the common data used to survey the path and to form the basis of geosteering in directional drilling operations.

Data Transmission

One of the problems that arise with LWD in contrast to the conventional wireline logging is the data transmission capacity. Wireline logging operations are performed by logging tools that are attached to a coaxial cable that provides the linkage between the subsurface equipment and the surface equipment for data transmission purposes. However in the case of LWD operations, the tools are a part of the bottom hole assembly which is in continuous rotating motion and there is no such cable present to transmit the data. Thus,

even with the recent advances in technology for gathering and storage of petrophysical and engineering data and relatively slow movement speed of LWD compared to conventional wireline logging, the real time data transmission becomes an important issue.

Data Compression Using Wavelets

Without waiting for new technological improvements, one method to transmit more real time information from downhole during LWD measurements is to compress the data and send more information to the surface using the same data transmission capacity. Application of wavelet transforms have been among the three important techniques used for data compression in LWD along with variable-length coding where fewer bits are assigned to frequent events and predictive coding where predictions are made based on previous occurrences.

In their reservoir characterization studies, Panda et al. (2000) had also showed that wavelet transforms were good tools for denoising the data and could be used for scale-up purposes without losing important information, however perhaps the most important work specifically in the area LWD data compression has been studies of Bernasconi et al. (1999) in which they accomplished compression of data from downhole measurements with up to a ratio of 15:1 with a very small signal degeneration using an algorithm based on the wavelet transform. This ratio was by far the best compared to the other data compression methods which were 2.1:1 for variable length coding and 1.65:1 for predictive coding. This method was based on data transmission using mud pulse telemetry but the advantage of wavelet transforms of being independent from the data telemetry method, similar algorithms may be used for data compression purposes with other telemetry methods for LWD which are acoustic, electromagnetic and continuous wave telemetry without major modifications

Geosteering

Geosteering conventionally describes the directional handling of the drilling activity towards a determined location based on geological interpretations. The goal of geosteering is to effectively place the well to maximize the contact to the pay zone, thus enhance the hydrocarbon production and to improve economics through maximizing the productive reservoir by hitting as many targets as possible. Introduction of LWD real time data collection has also had its applications in the topic of geosteering. With LWD tools getting located increasingly closer to the end of the bottom hole assembly, log data such as resistivity measurements have also been increasingly used for geosteering purposes in conjunction with conventional parameters such as weight on bit and rotary speed. However there is still some vagueness in geosteering using LWD data resulting from the location of the LWD tools as they can only be located some distance from the bit.

Other than their applications in signal compression, wavelets have also been noted for their ability to detect both transient and stationary behaviors of signals. Even the local instant discontinuities that remain indistinguishable when using the classical methods can be detected using wavelets (Fig. A.1) giving the exact instant when a signal changes as well as the amplitude of the change.

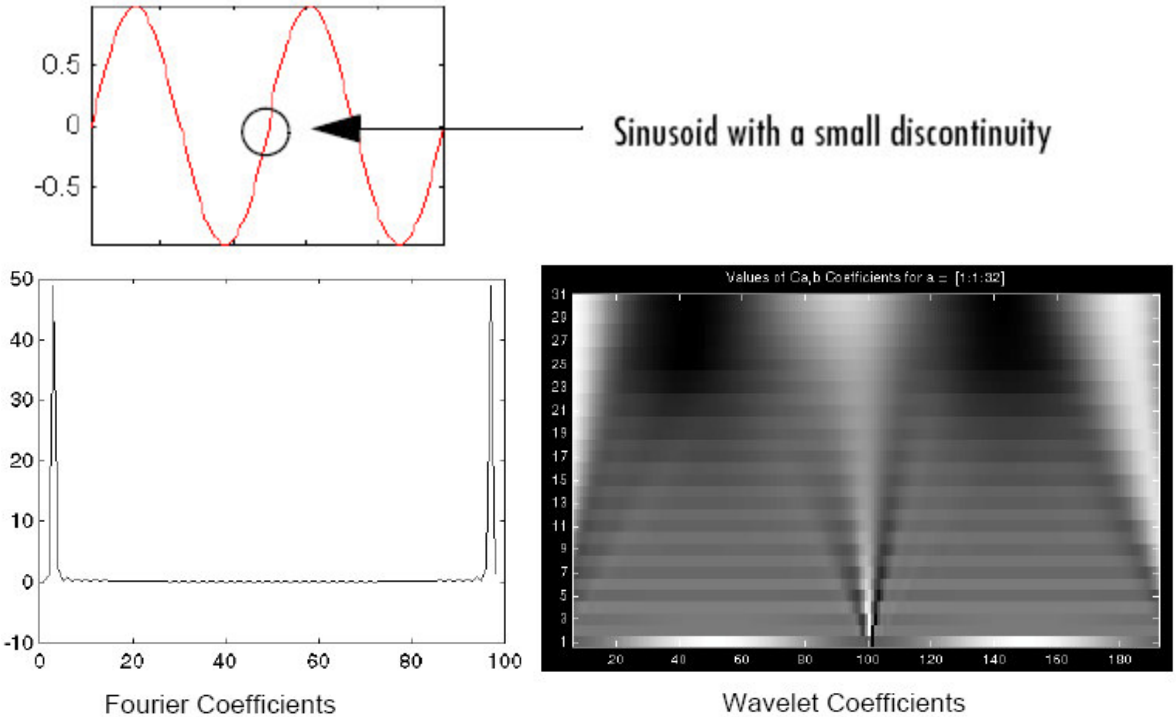

Figure A.1 Fourier coefficients and Wavelet coefficients for a sinusoidal signal with a small discontinuity (from Misiti et al., 2004).

Studies of wavelet analysis on MWD data may provide a faster observation for geosteering purposes that may overcome the uncertainty that arises as a result of the location of the LWD tools. Since MWD data gives information about a certain depth before the LWD tools does, important breakpoints in the data can be determined more rapidly by using the MWD data.

APPENDIX B

TOTAL ENERGY DIAGRAMS FOR MILANKOVITCH CYCLES

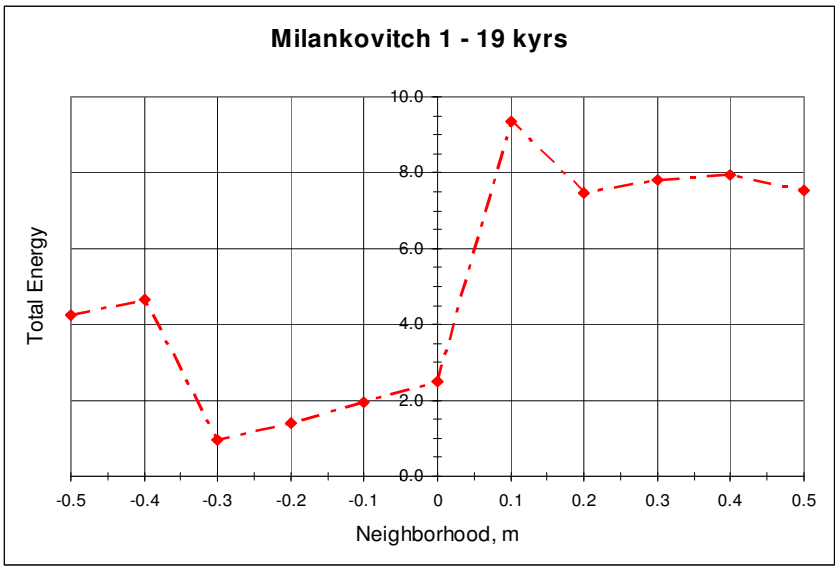

Figure B.1 Total energy diagram around ±0.5 m neighborhood of 19 kyr Milankovitch 1 depositional cycle thickness associated with the depositional rates.

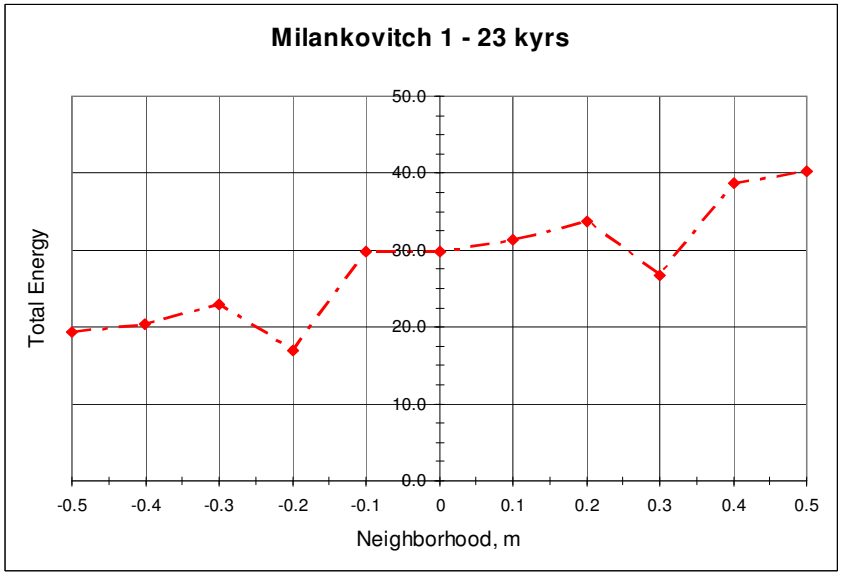

Figure B.2 Total energy diagram around ±0.5 m neighborhood of 23 kyr Milankovitch 1 depositional cycle thickness associated with the depositional rates.

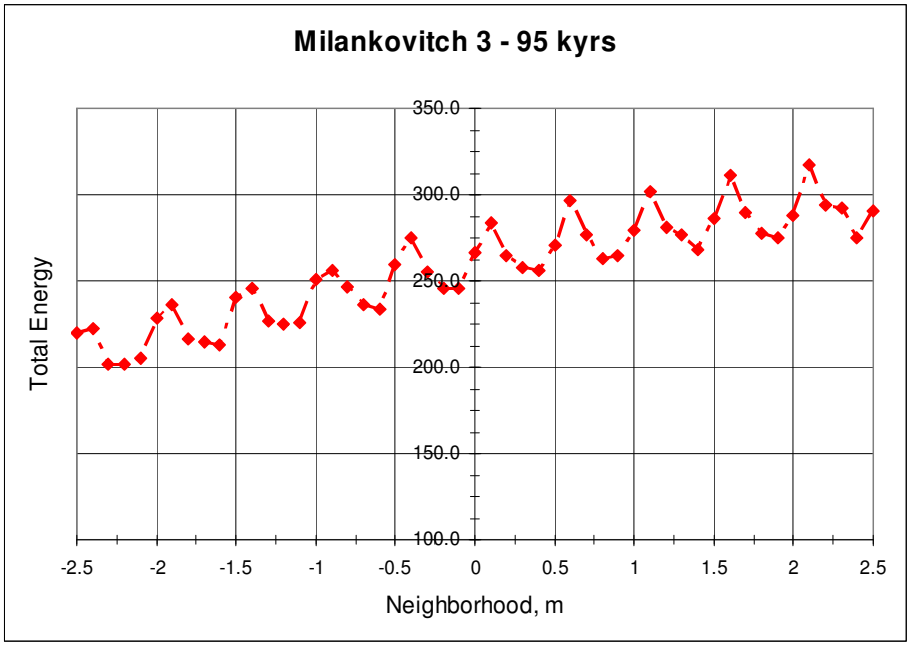

Figure B.3 Total energy diagram around ±2.5 m neighborhood of 95 kyr Milankovitch 3 depositional cycle thickness associated with the depositional rates.

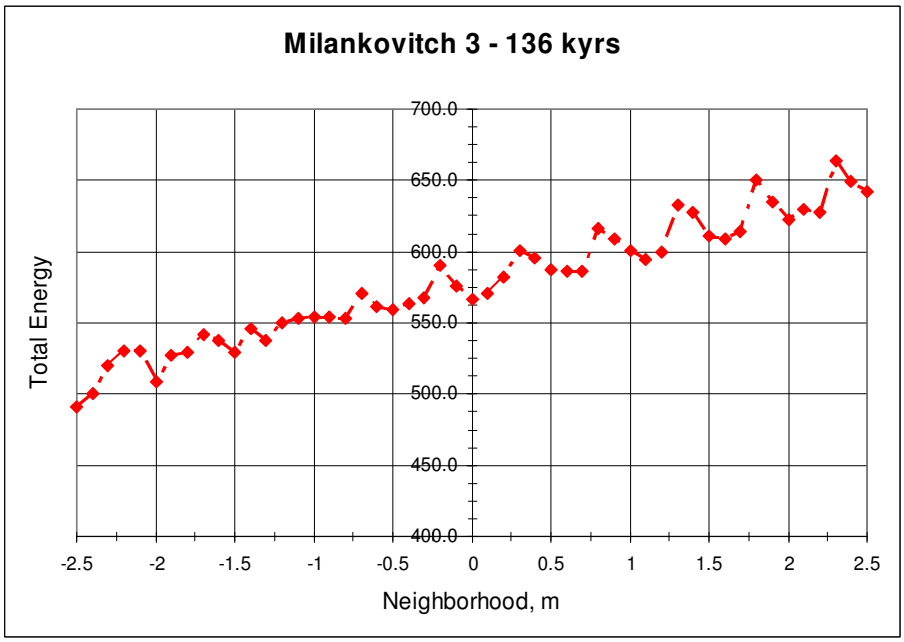

Figure B.4 Total energy diagram around ±2.5 m neighborhood of 136 kyr Milankovitch 3 depositional cycle thickness associated with the depositional rates.

VITA

Emre Doruk Tanyel was born in Ankara, Turkey on May 10, 1980. He received his B.S. degree in petroleum and natural gas engineering, in June 2001 from the Middle East Technical University, Turkey. In 2001 he started working for Petoil Petroleum and Petroleum Products Inc., Ankara, Turkey where he worked as a junior engineer to assist in designs of field operations until 2002. He started the M.S. program in petroleum engineering at Texas A&M in September 2003, and received his degree in August 2006. His permanent address is:

Ozvatan Sokak 24/1
Guzeltepe Mahallesi
Cankaya – Ankara, Turkey